MODELING OF PHOTOSYNTHETIC OSCILLATIONS OF INTERNAL CARBON DIOXIDE IN PLANT LEAF

MD RUHUL AMIN
M. Sc. Biotechnology and Genetic Engineering, Khulna University, Khulna, Bangladesh, 2007

A Thesis
Submitted to the School of Graduate Studies
of the University of Lethbridge
in Partial Fulfilment of the
Requirements for the Degree

M. Sc. BIOCHEMISTRY

Department of Chemistry and Biochemistry
University of Lethbridge
LETHBRIDGE, ALBERTA, CANADA

Dedication
To my parents.

Abstract

In photosynthesis, Rubisco catalyzes two alternative reactions: carboxylation and oxygenation of RuBP. The carboxylation reaction utilizes CO_2 in the chloroplasts, whereas the oxygenation reaction eventually leads to CO_2 production in the mitochondria. An irregular oscillation of the internal CO_2 concentration was observed in a previously published experimental study in a low CO_2 environment [Roussel *et al*., J. Plant Physiol. 2007, 164, 1188.], where it was hypothesized that photorespiratory CO_2 produced in the mitochondria may diffuse to the chloroplast and give rise to the oscillations. I built a compartmental model of the process with delay. I analyzed the model through a graphical analysis method and found that my model has the potential to oscillate, but only when there are delays. In addition, I found that the model displays both the regular and irregular oscillations at different parameter sets, but at unrealistic parameter values leading to unrealistic CO_2 concentrations.

Acknowledgements

The special thanks goes to my supervisor Dr. Marc R. Roussel for providing me the opportunity to pursue a Master's degree under his supervision. The support and guidance that he gave me help in boosting the smoothness and progress in this project. This thesis would not have been possible without his patience. I am highly indebted to him for his continued support, fruitful patience and helpful guidance.

I would like to thank both my committee members, Dr. Hans-Joachim Wieden and Dr. Larry Flanagan for their big contribution through valuable suggestions and feedbacks, which was really great indeed. I appreciate their co-operation.

I am grateful to the Department of Chemistry and Biochemistry and the School of Graduate Studies for their financial support and co-operation.

I would like to extend a special thanks to all of my lab members for thoughtful discussion during this period of my research journey. Last but not the least, I would like to thank my family members, specially my wife, Laila Mostahid Lubna, for encouraging me for this degree.

Table of Contents

List of tables:

List of Figures

Abbreviations:

CA: Carbonic anhydrase

FMN: Flavin mono-nucleotide

GGAT: Glutamate:glyoxalate amino transferase

GDC: Glycine decarboxylase

GLYR: Glyoxalate reductase

HT: Hexose translocator

PPT: Phosphoenolpyruvate/phosphate translocator

Rubisco: Ribulose-1, 5-bisphosphate carboxylase/oxygenase

RuBP: Ribulose-1, 5-bisphosphate

SGAT: Serine:glyoxalate amino transferase

SHMT: Serine hydroxymethyltransferase

TPT: Triose phosphate translocator

3PGA: Glycerate 3-phosphate

Chapter 1: Introduction

1. Introduction

"*I observed that plants not only have the faculty to correct bad air in six to ten days, by growing in it...but that they perform this important office in a complete manner in a few hours; that this wonderful operation is by no means owing to the vegetation of the plant, but to the influence of light of the sun upon the plant*". – Jan Ingenhousz.[1]

Photosynthesis is the principal process by which plants and some bacteria convert inorganic carbon to organic compounds and release oxygen into the atmosphere. In this process, sunlight energy captured by the chlorophyll pigments becomes usable chemical energy. Nowadays, the CO_2 concentration in the atmosphere is increasing dramatically due to excessive human activity.[2] Photosynthesis is the only process respectively to remove the CO_2 from and to release O_2 to the atmosphere. But photorespiration releases CO_2, and is a wasteful process as it reduces the efficiency of photosynthesis by removing carbon compounds from the Calvin cycle.[3]

The evolutionary origin of photorespiration from Cyanobacteria has been described.[4] When plants appeared on Earth, the O_2 content of the atmosphere started increasing, eventually reaching the present level of 21% from about 2%.[4] Intense photosynthetic activity in the Carboniferous period resulted in a short-term fall of the CO_2 and rise of the O_2 level. Later on, the existence of animals on Earth resulted in an increase of the CO_2 level.[2, 4] The current concentrations of CO_2 and O_2 in the atmosphere are about 390

μmol mol^{-1} and 209,700 μmol mol^{-1} (21%) respectively.[5,6] The CO_2 concentration will be in the range of 600-1000 μmol mol^{-1} by the end of 21st century.[5] A remarkable amount of research is under way at high CO_2 concentration levels to observe the consequences of high atmospheric CO_2 concentration on photosynthesis and photorespiration.[4,7] From the practical aspect, research at high CO_2 concentration is important to observe plant growth and other metabolic responses of plants in the presence of the expected increased CO_2 concentration. In contrast, research at low CO_2 could be crucial to disclose the evolutionary biochemistry of photosynthesis and photorespiration. Comparatively less research is going on to observe the consequence of low CO_2 containing environments. With this view in mind, an experimental effort was undertaken in a low CO_2 environment and irregular oscillations were observed.[8] To study this type of irregular oscillations, a sufficiently detailed model of the system was developed in this thesis.

In this chapter, a detailed biochemical review of the system is presented. In addition, the objectives of this thesis will be also discussed here.

1.2 Modeling background

In general, modeling can be defined as the extraction of the most important features of a system and the translation of these features into a metaphor, whether that is a reaction scheme, a diagram, a set of equations or something else altogether. Typically a set of equations of the corresponding system is generated following certain laws, for example a biochemical model can be developed following chemical and physical laws. In a biochemical or ecological context, often the final model takes the form of ordinary or

delay differential equations (ODEs or DDEs). The computer has been used for modeling since the early 1960s.[9] A number of theoretical and conceptual tools have been developed during this time, including numerical bifurcation analysis.[10] Mainly two kinds of software have been applied in modeling: general-purpose mathematical software and specialized biochemical modeling software.[9] An example of general-purpose mathematical software is Matlab,[9] which works with a set of differential equations. WinScamp[11] and Gepasi[12] are examples of specialized modeling software. The researchers start by working with a set of reactions; for example, in a biochemical pathway, they start by describing enzyme catalysis or transport processes. Later, they uncover appropriate parameters value from the literature when possible, otherwise parameters may be estimated. Once the set of reactions and the parameters are chosen, the researchers are in a position to produce results. The first attempt is likely to fail due to missing an important step or steps of the system or by choosing a wrong parameter; this step is known as constructive interrogation. If the model works well and produces at least some of the expected or characteristic phenomena of the system under study, this stage is called analytic interrogation.[9] One schematic working pattern of modeling has been suggested that consists of the above-mentioned alternative steps[9] (fig 1).

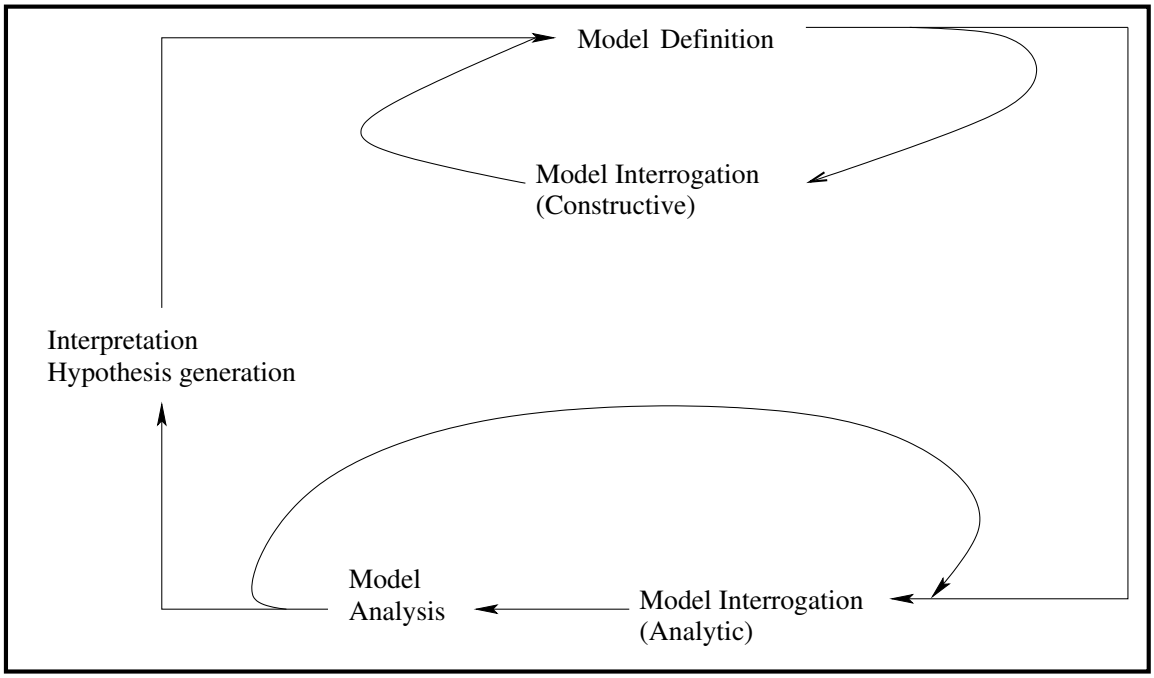

Figure 1: Schematic diagram of modeling (adapted from ref. 9)

There are several ways to estimate a parameter value when a literature search has been unsuccessful. The researcher can find parameter values for closely related processes. For an example, if the researcher is looking for the kinetic parameters of an enzyme in a particular organism that is unavailable, they can look for parameters for the same enzyme from a different organism. Sometimes it is possible to estimate a parameter value from other available data, or at least to find the upper and lower limits of the parameter value. In some cases, it is possible to fit a model to the data for estimation of the parameters. If nothing works, the parameter becomes a free parameter, whose value can be varied during model interrogation.

1.3 Oscillations in photosynthesis

A considerable amount of interest has been shown in studying the photosynthetic oscillations in the last couple of decades.[13, 14] Major studies in this field consider the oscillations of O_2 evolution and CO_2 uptake in photosynthesis,[13] the oscillations of photosynthetic rates,[15] and the oscillations in photosynthetic metabolites.[16] Both experimental studies[8, 13-15] and mathematical modeling[16-17] have been applied to study this phenomenon. But the understanding of this phenomenon is not complete yet. Oscillations may be judged as an indication of important regulatory processes involved in photosynthesis. Researchers are still trying to find out the important regulatory mechanism or mechanisms behind these oscillations. Recently, a similar type of attempt was made by Roussel and coworkers.[8] To my knowledge this is the only experiment of this type performed in the low CO_2 environment. The tobacco plant leaves were transferred from 350 $\mu l\ l^{-1}$ to 36.5 $\mu l\ l^{-1}$ of atmospheric CO_2 concentration. An irregular type of oscillation of internal CO_2 concentration was observed (fig 2). The authors hypothesized that the irregular oscillations may arise from switching between photosynthesis and photorespiration.[8] In theory, the oscillations can occur if a feedback mechanism exists.[18] In this case, the photosynthesis process is fed by CO_2 released from the photorespiration process that is coming to the reaction site later. It has also been suggested that the oscillations may arise when the substrate concentration is sufficiently lower than the enzyme concentration.[18] As the substrate is at a low concentration, it can run down if the reaction continues. The same situation occurs in photosynthesis, where the Rubisco (ribulose 1,5-bisphosphate carboxylase/oxygenase, an enzyme of the Calvin cycle) concentration is in the milimolar range and the CO_2 concentration is in the

micromolar range.

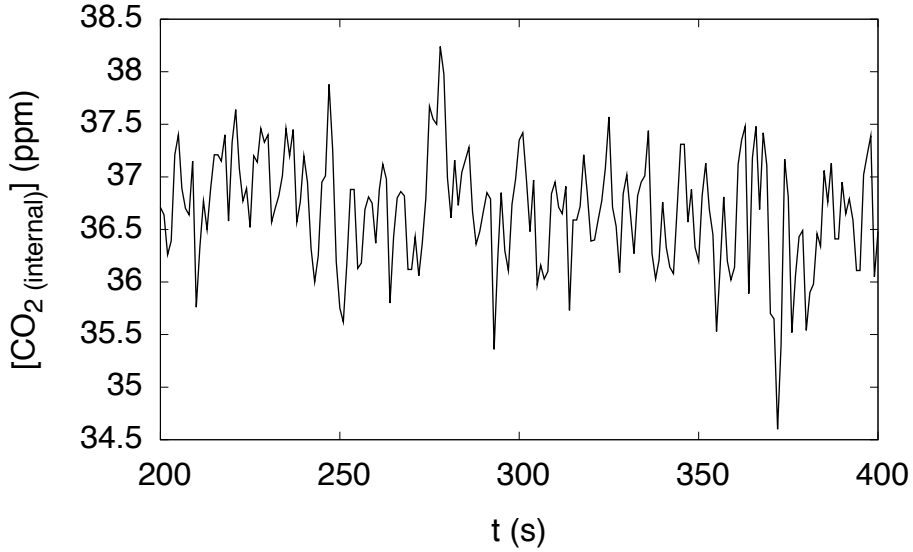

Figure 2: Irregular oscillations observed in the experiment

In this thesis, a model of the process is developed. Compared to the model of Dubinsky and Ivlev,[17] my model contains much more biochemical detail. For example, the diffusion of O_2 and CO_2 and the solubility of O_2 and CO_2 in different cellular environments (e.g. inside and outside of a cell or cell compartment) were not considered in their model. On the other hand, these realistic physiological properties of plant leaves are included in my model. The glycolate pathway of photorespiration in releasing CO_2 in mitochondria is also included in my model by introducing a delay term.

1.4 Photosynthesis and photorespiration

In photosynthesis, Rubisco catalyses the reaction of CO_2 and RuBP (Ribulose-1,5-bisphosphate), producing two molecules of glycerate 3-phosphate (3PGA). In

photorespiration, Rubisco also catalyses the reaction of O_2 and RuBP, producing one molecule of 3PGA and one molecule of P-glycolate (fig 3). About one-fourth of the total energy captured through photosynthesis is released by photorespiration.[4-5] In other words, photorespiration is an alternative process to photosynthesis, which unravels part of the photosynthetic work. That is why the role of photorespiration is controversial. Some scientists suggest that it is a wasteful process with no benefit to the plant, whereas others suggest that it might have some cryptic benefits.[5] Photorespiration slows down photosynthesis under certain stressful conditions (intense light, drought stress, etc.) and protects photosynthetic organelles from damage.[5] It is also reported that it plays an important role in nitrate (NO_3^-) assimilation in plant shoots.[5]

Rubisco has a strong affinity for O_2 as well as for CO_2. The specificity of Rubisco for CO_2 vs O_2 is about 88:1 if CO_2 and O_2 are present in equal molar concentrations in the stroma.[7] But in the cell under normal atmospheric conditions the concentrations are in a 23:1 O_2:CO_2 ratio. Hence, the CO_2 concentration in the cellular compartment is typically low and the oxygen concentration in the cell is much higher. These gases enter into leaf mesophyll tissue by diffusion.[19] The measurement of CO_2 concentration in the leaf has been done by gas-exchange measurements.[8, 20-21] The substrates CO_2 and O_2 react with Rubisco in a competitive manner. The O_2 substitutes for CO_2 when the CO_2 concentration goes down, leading to photorespiration, producing 3PGA and P-glycolate. The 3PGA directly enters into the Calvin cycle but P-glycolate cannot.

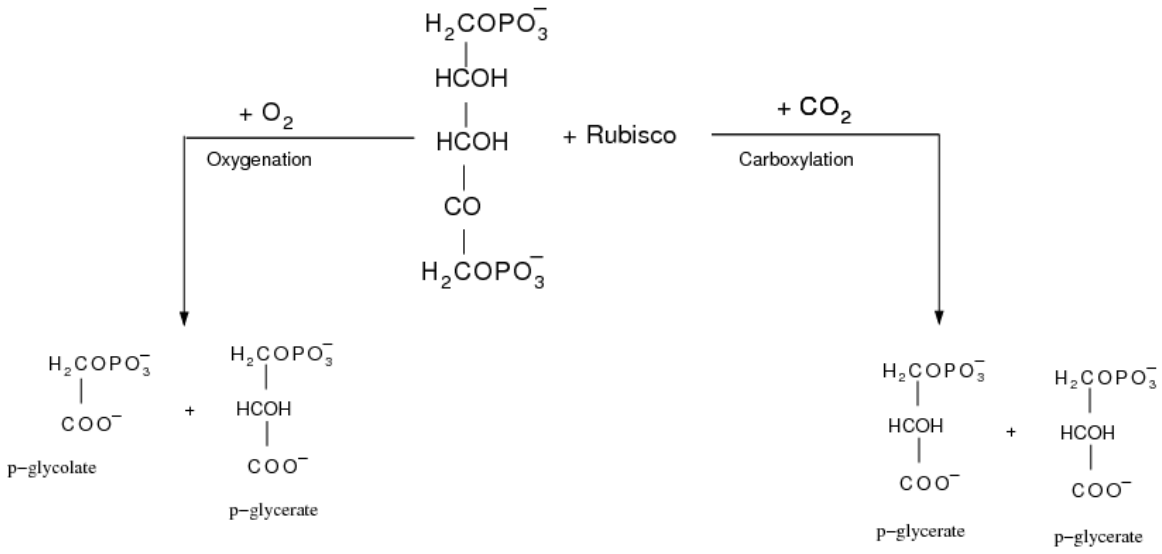

Figure 3: The carboxylation and oxygenation of RuBP (adapted from Ref. 22)

Moreover, accumulation of phosphoglycolate is toxic for the plant. Phosphoglycolate can be converted to 3PGA through the photorespiration cycle and 3PGA can enter into the Calvin cycle, relieving plants from this stress. Conversion goes through eight complex enzymatic reactions and those reactions are occurring in four distinct compartments: the chloroplast, the peroxisome, the mitochondrion and the cytoplasm.[4] One molecule of CO_2 is produced during the conversion of P-glycolate to P-glycerate. It has been suggested that this photorespiratory CO_2 can be involved in the oscillatory feedback mechanism.[8] An alternative hypothesis has also been reported that could contribute to increase the CO_2 stoichiometry under stress[23] (fig 4).

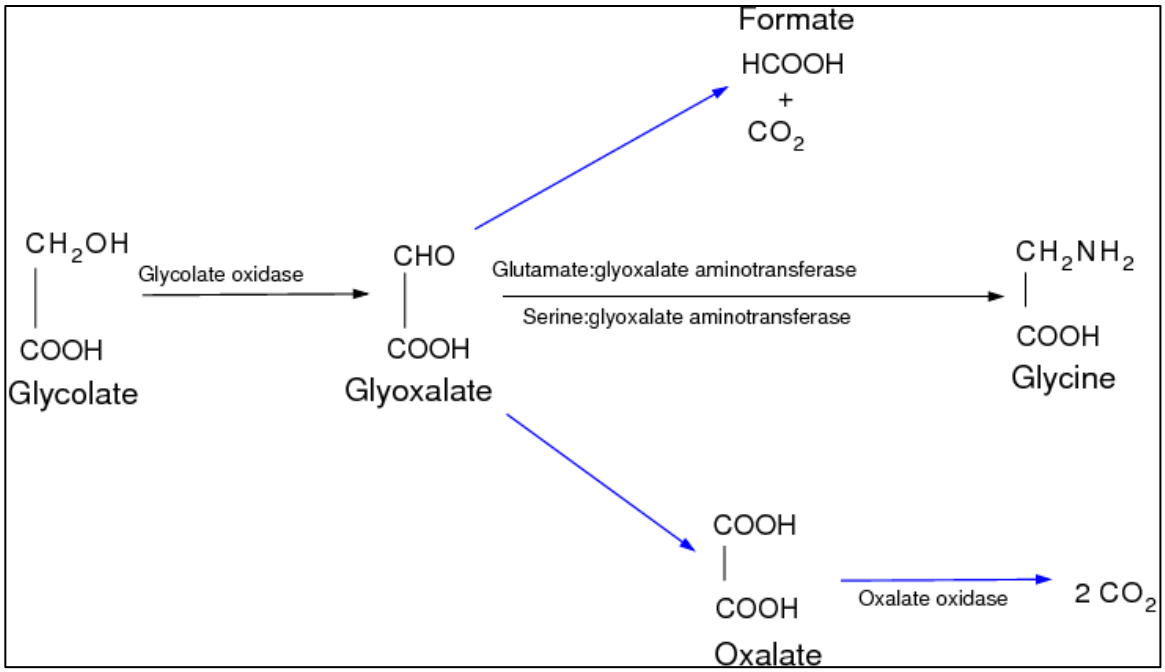

Figure 4: Alternative pathway to produce CO_2 (adapted from Ref. 23)

1.5 Rubisco

Rubisco has mainly two structural forms, namely form I and form II. Form I of Rubisco is commonly found in plants, algae, cyanobacteria, autotrophic bacteria, and form II is in dinoflagellates and in obligate anaerobic bacteria. Form I Rubisco consists of eight large (chloroplast rbcL gene) and eight small (nuclear rbcS) subunits. The chloroplast rbcL gene encodes the 55-kDa large subunit and the nuclear rbcS gene is responsible for the 15-kDa small subunit. In contrast, form II Rubisco has only large subunits, and lacks the small subunits.[24] The catalytic efficiencies of forms I and II of Rubisco are low and high, respectively.[24] Another two types of Rubisco, form III and form IV, have also been reported recently.[25] Form III is common in archaebacteria as a dimer and has a high catalytic constant. Form IV of Rubisco is composed of Rubisco-like protein, but it

does not catalyze the reaction of CO_2 with RuBP; rather it participates in the methionine salvage pathway.[25]

Rubisco is said to be the most abundant, important, as well as inefficient enzyme on Earth because of its low catalytic rate.[24] The catalytic efficiency of this enzyme is low in terms of k_{cat} (2-12 s^{-1}) and k_{cat}/K_m ratio (5-40 x 10^{-4} M^{-1} s^{-1}). This low efficiency necessitates the large amount of Rubisco present in leaves to maintain the proper photosynthesis rate. The amount is calculated to be about 50 percent of leaf protein.[22] The concentration of this enzyme in the stroma of the chloroplast is about 0.2 g mL^{-1}. The kinetic constants of Rubisco vary from species to species. The Michaelis-Menten constant for the carboxylase reaction (K_c) ranges between 13-26 μM and for the oxygenase reaction (K_o) from 28-64 μM.[26]

Recent studies have described the catalytic cycle of Rubisco following three steps: carbamylation, structural changes and CO_2/O_2 specificity.[22] The catalytic activity depends on two cofactors; the metal ion Mg^{2+} and a CO_2 molecule. The CO_2 (distinct from the CO_2 molecule that participates in the reaction as a substrate) binds with the enzyme (E), which forms the EC complex, and then Mg^{2+} binds with the EC complex leading to the ECM complex (fig 5). The binding step of CO_2 is described as carbamylation.[22] Carbamylated Rubisco with Mg^{2+} is described as active, or catalytically competent, Rubisco.

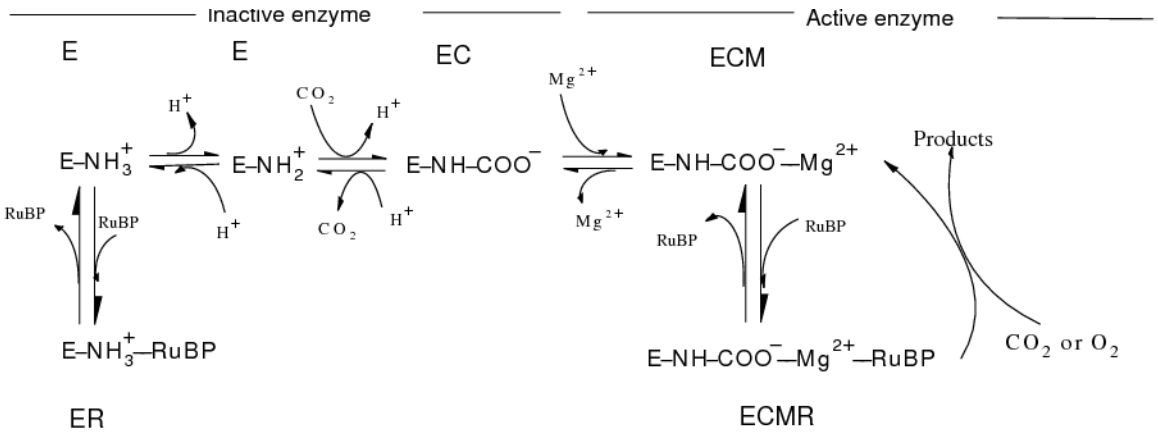

Figure 5: Sequential steps in activation of Rubisco (adapted from Ref. 22).

Upon carbamylation, the side chain of the lysine residue (K201) changes from a positive charge to a negative charge and Mg^{2+} binds to one of the carbamino oxygen atoms.[22] This explains why metal binding actually occurs after carbamylation takes place. Carbamylation causes a pH change as two protons are released during this process.[27]

A small conformational change occurs in the Rubisco active site after carbamylation. A larger conformational change occurs when RuBP binds with the Rubisco active site, about a 12-Å shift of the α/β-barrel of loop 6 from an open to a closed conformation.[22] In crystallographic studies, the active site residue position changes upon carbamylation and Mg^{2+} binding and these types of changes are common in the ECM and ECMR complexes (fig 5).[22]

It has been proposed that Rubisco reacts with the substrates in a specific ordered sequence.[28] The binding of substrate CO_2 or O_2 determines the overall reaction rate of the process. Binding of substrate CO_2 or O_2 occurs with a probability that is determined by

the kinetic constants of Rubisco and by the atmospheric pressure of gases. The selectivity between CO_2 and O_2 is determined by the specificity factor.[22] The relative specificity ($S_{c/o}$) is determined by a ratio of the V_{max}/ K_m values:

$S_{c/o}= (V_c/K_c) / (V_o/K_o)$,

where $V_c= V_{max}$ for carboxylation, $V_o= V_{max}$ for oxygenation, $K_c= K_m$ for carboxylation, $K_o= K_m$ for oxygenation.

The specificity factor varies with the metal ion activating Rubisco. When the activating divalent metal is Mg^{2+}, the specificity factor for CO_2/O_2 is 10-25 times greater compared to Mn^{2+}. It has also been reported that the specificity factor is different for the different forms of Rubisco.[29]

The metal-stabilized carbamate state enables the active site to bind with the RuBP before binding with one of the gaseous substrates CO_2 or O_2. The RuBP forms an intermediate enediol in the active site. The CO_2 and O_2 molecules used in the carboxylase and oxygenase reaction respectively compete for the enediol form of RuBP. If either of the substrates reacts with the enediol, then the enzyme is committed to form products.[30]

1.5.1 Rubisco activation and inactivation

Rubisco activation and deactivation are relatively slow, in contrast with other photosynthetic carbon reduction cycle processes.[31] Characteristic times of about 4-5 minutes have been reported for activation and about 20-25 minutes for the inactivation process.[32] Fluctuating light has an intense effect on this slow activation and relatively

slower inactivation process of Rubisco, and ultimately on the CO_2 assimilation. It has also been proposed that the activation and deactivation rates of Rubisco are not very different between species.[31] A linear dependency of Rubisco activation on Rubisco activase content has been reported in mutant *Arabidopsis* and transgenic tobacco. A slow rate of photosynthesis with low Rubisco activase content has been also described.[33-34] These results suggest that the activase has some effect on the photosynthesis rate in the steady state. It has been proposed that tobacco leaves have about 40-100 mg (1-2% of leaf soluble protein) activase.[20]

Rubisco can be fully carbamylated and active at ambient CO_2 concentration and high light.[32] When RuBP was present in *in vitro* experiments, RuBP blocked the carbamylation by binding tightly to the non-carbamylated site.[29] Rubisco activase has been reported to break down the tight binding between the RuBP and Rubisco.[35] ATP hydrolysis is required for the activation of Rubisco activase. Active activase eliminates the RuBP from the non-carbamylated Rubisco sites, enhancing the carbamylation.[36] A model has been proposed for the mode of action of activase.[32] In that model, it has been proposed that activase is activated by ATP hydrolysis, which can bind to Rubisco in a closed conformation (enzyme-RuBP complex, fig 6). After binding it changes conformation from closed to open and releases RuBP with inactive activase (fig 6).

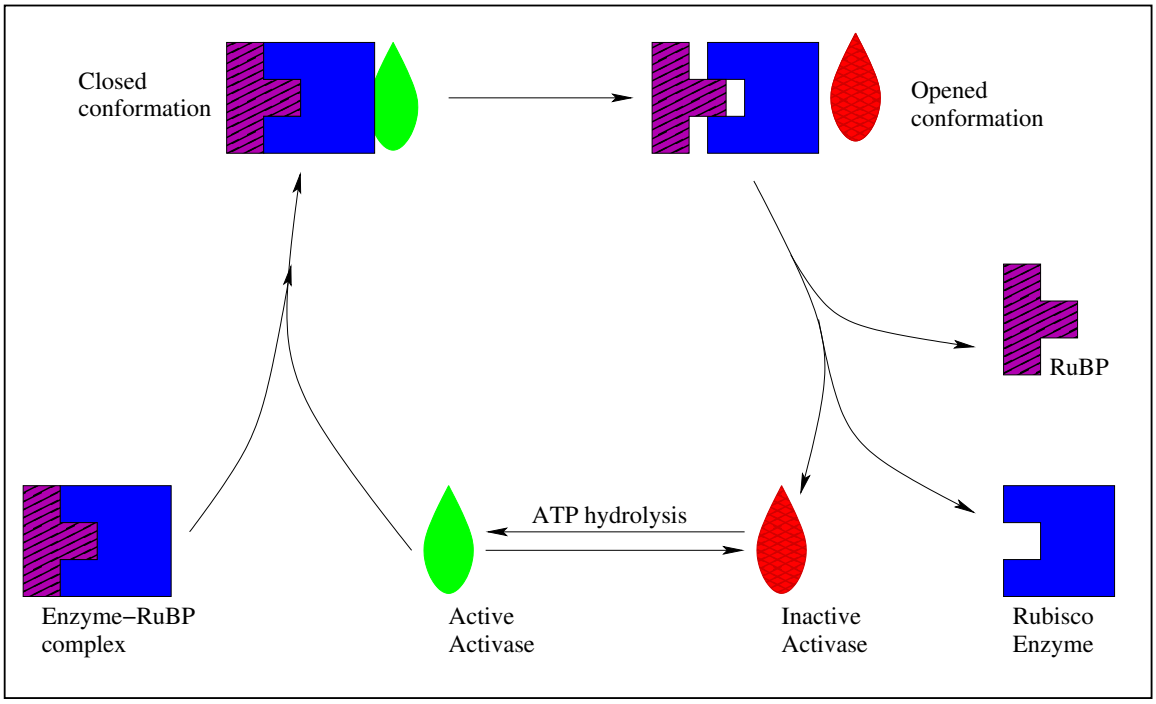

Figure 6: The model for activase function (adapted from Ref. 32).

1.5.2 Kinetic constants *in vivo* and *in vitro*

It has been shown that estimates of kinetic constants *in vitro* for Rubisco are different in different species (Table 1). Extraction and purification make *in vitro* estimates of kinetic constants questionable. So, *in vivo* estimation of K_c and K_o is preferable. *In vivo* measurements of K_c and K_o fall in the range of the *in vitro* estimates, but at the bottom end of the range.[32]

Several studies have shown that the rate of carboxylation depends on the RuBP concentration.[37-38] The Michaelis-Menten constant K_m for RuBP is about 20 μM.[39] The chloroplast has a large pool of about 10 mM for both RuBP and PGA. The concentration of Rubisco active sites has been reported as 1-4 mM *in vivo*.[32]

Table 1: *In vitro* measurement of Rubisco kinetics constants in different species at 25^0 C (data from ref. 32)

Species	**K_c (μM)**	**K_o (μM)**	$V_{O\max}/V_{C\max}$	**$S_{c/o}$**
Glycine max	9	430	0.58	82
Nicotiana tabacum	11	650	0.77	77
Oryza sativa	8	335	0.33	128
Lolium perenne	16	500	0.38	80

This active-site concentration is enough to bind a significant amount of RuBP. The carboxylation rate increases linearly until the RuBP concentration equals the active Rubisco site concentration and saturates when RuBP exceeds the active Rubisco site concentration.[40] Some studies have suggested that about 1.5-2 times more RuBP is required than the Rubisco site concentration to saturate.[37-38] It has been reported that Rubisco activation is dependent on CO_2 and Mg^{2+} concentrations *in vitro*.[41] In contrast, dependence on CO_2 is not observed *in vivo*.[32] It has been hypothesized that RuBP and activase maintain the Rubisco activation state *in vivo*.[32]

1.6 Photorespiratory pathway

The chloroplast is the center for photosynthesis and P-glycolate is produced in the chloroplast by photorespiration (fig 7). Later P-glycolate is hydrolyzed to glycolate by phosphoglycolate phosphatase in the same compartment. Phosphoglycolate phosphatase

has been reported as a dimer of 32 kDa and it has a low K_m value, below 100 μM. So, the hydrolysis of P-glycolate by phosphatase is very efficient. The glycolate is transported from the chloroplast to the peroxisome. Export from the chloroplast occurs through a transporter channel. This transporter has a similar affinity for glycolate, glyoxalate, D-glycerate and D-lactate.[42]

Protein channels are responsible for the uptake of biomolecules into the peroxisome as the presence of a porin has been reported in the membrane of this organelle. Glycolate is transported to the peroxisome from the chloroplast in exchange for glycerate, which is the ultimate product of the photophosphorylation cycle. The amount of glycerate returning would be about 50% of the total amount of glycolate released from the chloroplast. Transport of glycolate and glycerate takes place by antiport of each other or H^+ symport or OH^- antiport.[42] In the peroxisome, the conversion of glycolate to glyoxalate is catalyzed by glycolate oxidase in an irreversible manner with a K_m value of 0.25-0.4 mM.[43] In this reaction, simultaneous reduction of flavin mono-nucleotide (FMN) takes place, which in turn is reoxidized with oxygen to produce hydrogen peroxide. The glycolate oxidase is a tetramer of subunits of 37-40 kDa. The subunit contains an eight-fold α/β barrel motif analogous to the FMN domain, which is common in other FMN-containing enzymes.[42]

The glyoxalate is converted to glycine by two alternative reactions in a 1:1 ratio. Two enzymes have been reported for the catalysis, namely serine:glyoxalate amino transferase (SGAT) and glutamate:glyoxalate amino transferase (GGAT). SGAT is a dimer of

different subunits of 45 kDa and 47 kDa.[44] GGAT also consists of two subunits and the molecular weight of this enzyme is 98 kDa. Serine is the amino donor and glyoxalate is the amino acceptor when the conversion is catalyzed by SGAT. The reaction catalyzed by SGAT is almost irreversible. The K_m values for the amino donor and acceptor are 0.6-2.7 mM and 0.15-4.6 mM, respectively.[42] In contrast, the amino donor is less precise when conversion is catalyzed by GGAT and the reaction is also reversible. In GGAT catalysis, 2-oxoglutarate is the amino acceptor when alanine is the amino donor[45] and glyoxalate is the amino acceptor when glutamate is the amino donor. The K_m values for glyoxalate or 2-oxoglutarate and glutamate or alanine are 0.15 mM and 2-3 mM, respectively.[42]

Glycine enters into the mitochondria (fig 7) once released from the peroxisome through the protein channels. Again, two enzymes are playing a crucial role in catalysis, glycine decarboxylase (GDC) and serine hydroxymethyltransferase (SHMT) to form serine, CO_2 and NH_3. Glycine decarboxylase consists of four protein components (P, H, T and L-protein, fig 8) and catalyzes the reaction of glycine to form CO_2 and NH_3. It has been also reported that catalytic efficiency of glycine decarboxylase depends on the physical proximity of active sites and the availability of substrates from subsequent reactions.[46] The left-over methylene carbon of glycine is attached to tetrahydropteroylpolyglutamate ($H_4PteGlu_n$) to form methylene-tetrahydropteroylpolyglutamate ($CH_2H_4PteGlu_n$). SHMT catalyzes the reaction of a second glycine molecule with $CH_2H_4PteGlu_n$ to produce serine. Two molecules of glycine enter into the mitochondria and one molecule of serine leaves the compartment.[42]

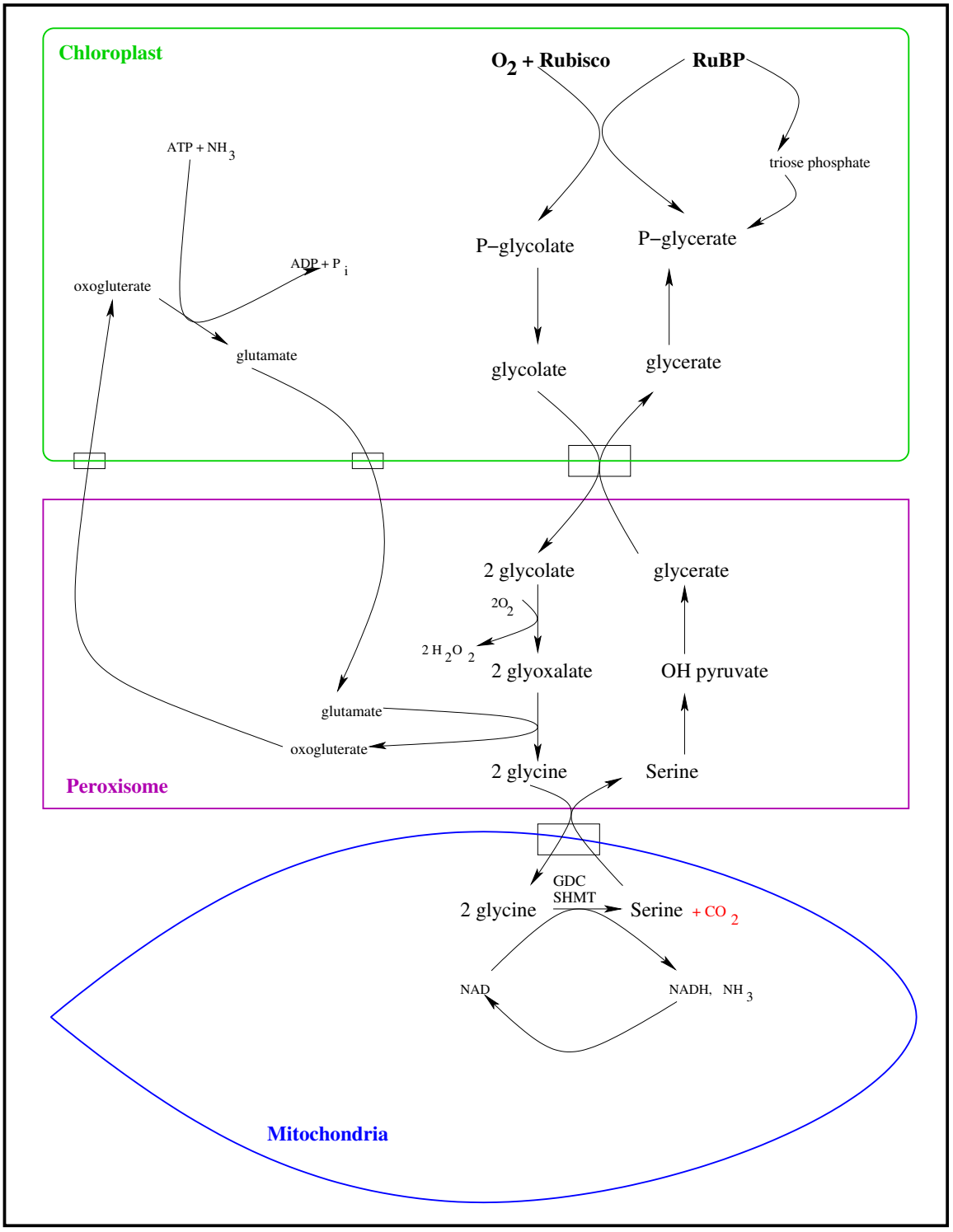

Figure 7: Photorespiratory pathway (adapted from Ref. 36).

Glycine is the end-product of the photorespiration pathway, and photosynthesis provides triose phosphate, which can be converted to pyruvate or oxaloacetate in the cytosol. All of these are mitochondrial substrates that can be oxidized in this compartment. These substrates can be exported from the chloroplasts to the mitochondria over a time scale varying from seconds to minutes. It has been reported that approximately 15-20 s is needed to release mitochondrial CO_2 in tobacco after the oxygenation reaction has occurred in the chloroplasts.[47]

Serine reaches the peroxisomal matrix from the mitochondria. Serine is converted into hydroxypyruvate by SGAT enzyme (same enzyme as described above) in a reaction that is virtually irreversible and does not have a feedback effect on its own synthesis. It has been reported that the concentration of serine in mitochondria is important as it regulates glycine decarboxylation. Binding of serine and glycine to the P-protein is competitive (K_i of serine is 4 mM; K_m of glycine is 6 mM) and that is why release of serine from the mitochondria is a vital step for glycine decarboxylation. Since only one molecule of serine is produced from two molecules of glycine, then the serine:glyoxalate aminotransferase (SGAT) converts fifty percent of glyoxalate into one molecule of glycine. Another molecule of glycine is produced from the remaining fifty percent of the glyoxalate by GGAT.[42]

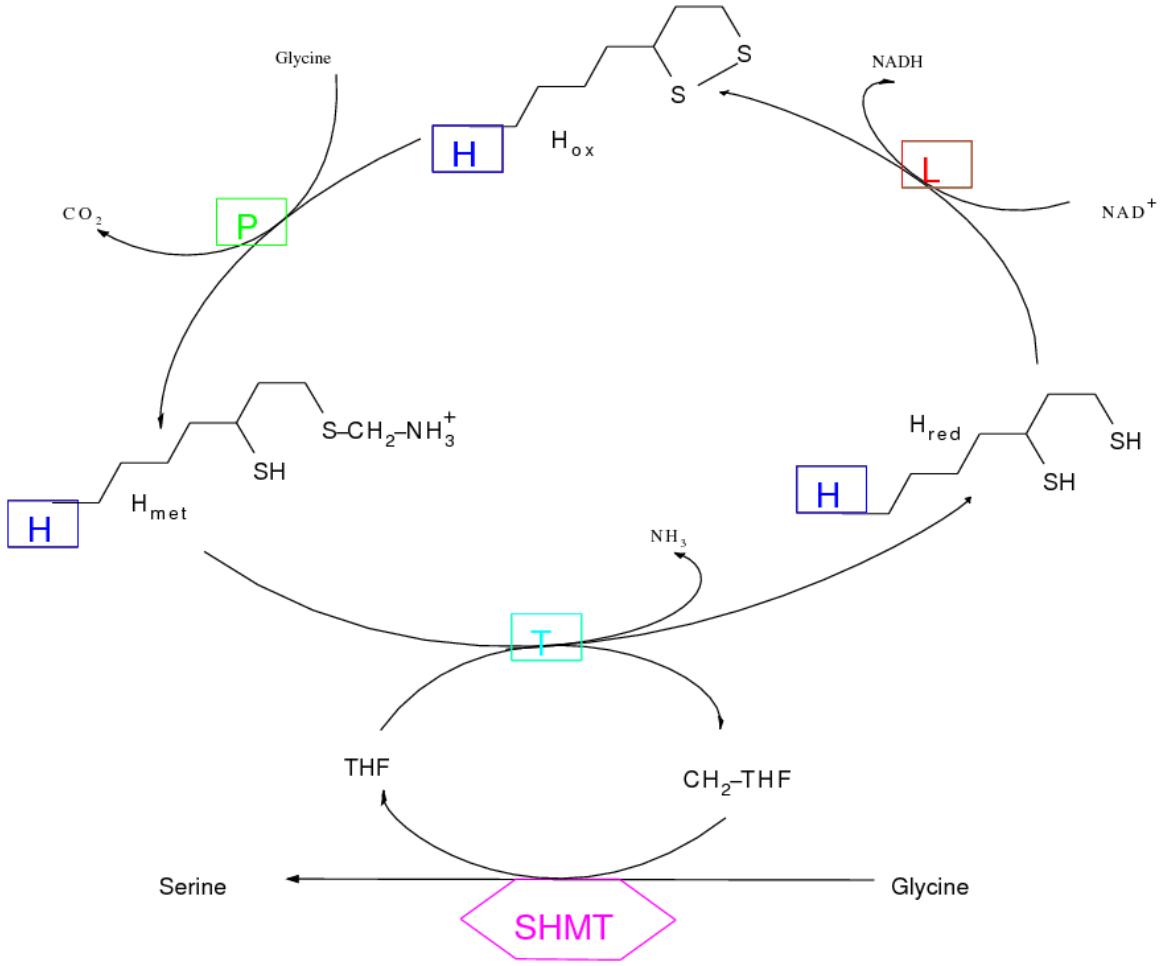

Figure 8: Sub-components of glycine decarboxylase (adapted from Ref. 48).

Hydroxypyruvate is reduced to glycerate by NADH dependent hydroxypyruvate reductase. The K_m value for NADH is 6 μM. When glyoxalate is used as an alternative substrate, this enzyme is known as glyoxalate reductase (GLYR). It has a much larger K_m value for glyoxalate (5-15 mM) compared to hydroxypyruvate (62-120 μM).[43] That is why it has been suggested that glyoxalate reductase does not have a crucial role under normal physiological conditions. It could play an important role under stress conditions, when glyoxalate leaks into the cytosol from the peroxisome.[49-50] Hydroxypyruvate reduction in the cytosol has been reported in barley mutants of peroxisomal

hydroxypyruvate reductase.[51] Both chloroplast (GLYR2) and cytosolic (GLYR1) genes have been reported in *Arabidopsis*.[23]

1.7 Transporters in the chloroplast

The chloroplast has at least two translocators that are involved in the transport of biomolecules. The triose phosphate translocator (TPT) exports triose phosphates and 3-phosphoglycerate (3PGA) from the chloroplast into the cytosol and imports phosphate ions. TPT is a dimer consisting of identical subunits and it was first isolated from spinach leaf.[52] It has been proposed that *Arabidopsis*, pea, potato, maize and tobacco all have similar translocators.[53] It has about 80 amino acid residues.[54] A ping-pong type reaction mechanism running in reverse has been described for this translocator. It has been proposed that the second substrate will transport in the opposite direction after the first substrate has been transported and has left the transport site alone.[52] The unidirectional transport of phosphate has been reported in intact chloroplasts with a lower V_{max} compared to antiport. That is why it has been proposed that the former transport mechanism may be different from antiport mode, and may involve a voltage-gated ion channel as well as an antiporter. The second transporter is the hexose translocator (HT) that exports glucose and the products from starch breakdown. Another type of phosphate transporter has been reported, named PPT (phosphoenolpyruvate/phosphate translocator).[53] The presence of an exchangeable substrate within the compartment is mandatory for the activity of both types of phosphate transporters (antiport systems).

1.8 Objectives

In this thesis, a reasonably detailed biochemical model of photosynthetic oscillations will be developed. A mathematical analysis will be performed to test whether the model has the potential to oscillate or not. Then we will analyze the model by computer simulations. The objectives of studying this phenomenon can be divided into two categories: one is a short-term and another is a long-term objective. The short-term goal of this thesis is to verify the hypothesis (discussed in section 1.3) made in the experimental paper,[8] i.e. is it possible to regenerate the irregular oscillations in low atmospheric CO_2 (36 $\mu l\ L^{-1}$) with a model based on that hypothesis? And the long-term goal is to shed light on the regulatory mechanism (or mechanisms?) responsible for producing the observed phenomenon.

Chapter 2: Model description

2.1 Introduction

The processes of photosynthesis and photorespiration are spread over several compartments. We built a compartmental model of these coupled processes. Nowadays, compartmental modeling is an important tool in analyzing the dynamic nature of biological processes and is useful in describing the transportation of chemical components among different compartments. Ecological and physiological systems are two other examples where compartmental models are used. In physiology, oxygen could be the chemical component and different organs of the body could be the compartments. The equations are derived for every compartment following certain conservation laws.

2.1.1 Leaf anatomy

Figure 9 shows most of the compartments of a leaf. Both the upper and lower sides of a leaf have an epidermis. The epidermis is covered by a waterproof cuticle. There are many pores, called stomata, present in the epidermal layer of each leaf. Both the entry of CO_2 and exit of O_2 and H_2O are controlled by the opening and closing of the stomata via the action of a pair of guard cells associated with each stoma. The mesophyll tissue is in between the two epidermal layers. Further, mesophyll tissue can be divided into two classes: palisade and spongy mesophyll tissue. Both types contain chloroplasts. The palisade mesophyll cells are beneath the upper epidermis and closely packed. One of these cells can be 80 μm long and can contain about sixty chloroplasts.[48] The spongy mesophyll cells are positioned between the palisade mesophyll cells and lower epidermis.

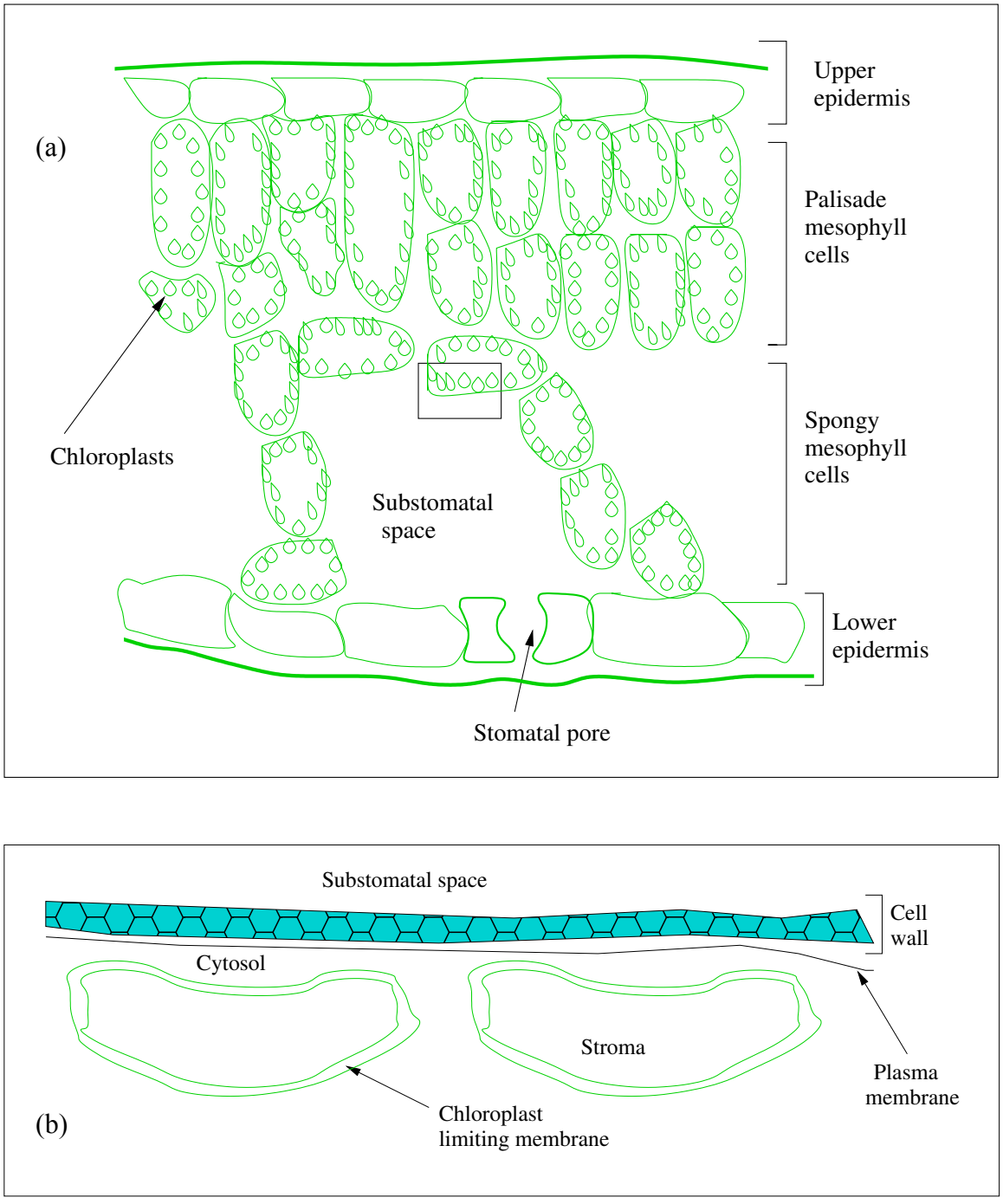

Figure 9: (a) Schematic presentation of various types of cells in a leaf. (b) Closeup of box from panel (a) showing the compartments available for the diffusion of CO_2 and O_2 (adapted from Ref. 48).

These cells are rather spherical, are about 20 μm in radius and can contain about forty chloroplasts per cell.[48] The surface areas of both types of mesophyll cells are exposed to the intercellular air space.

2.1.2 Diffusion and transport of CO_2 and O_2

Diffusion is the process by which net movement of substances occurs from the high to the adjacent low concentration region. Diffusion in plants happens in both gas and liquid phases. For an example, diffusion is the mechanism for O_2, CO_2 and H_2O transport in the surrounding air and within leaves. The CO_2 diffuses from the atmosphere through open stomata to the cell surface of the mesophyll cells. The O_2 travels in the same way. Water vapor evaporates from the cell walls of mesophyll cells and moves to the stomata through diffusion, and from there diffuses into the atmosphere. The diffusion coefficients of these three gases in air are all of the order of 10^{-5} m^2 s^{-1} (at 20^0 C and standard atmospheric pressure).[48] The diffusion coefficient for a small solute is about 10^4 times smaller in liquid phase than in the gas phase,[48] because more intermolecular collision occurs per unit time in liquid phase than in gas phase. In animal tissues, diffusion of O_2 and CO_2 is slow as most cells are floating in fluids, but in plant tissues the diffusion of these gases is faster due to presence of intercellular air spaces in leaves. Moreover, molecules with higher molecular weights tend to have lower diffusion coefficients. Thus CO_2 has a lower diffusion coefficient than O_2 in the gaseous phase.[48]

2.2 Model description

Figure 10 shows the key processes considered in our model. It is a delayed ordinary differential equation (ODE) model.[55] Atmospheric CO_2 and O_2 diffuse into the cytoplasmic space of mesophyll tissue through the substomatal space. Cytoplasmic CO_2 and O_2 diffuse into the chloroplast where they can respectively participate in the carboxylase and oxygenase reactions catalyzed by Rubisco. Rubisco can be found in many states in a plant cell.[24] Since the model has been built to reproduce the experimentally observed photosynthetic oscillations, the enzyme Rubisco (E) is considered as an active holo-enzyme in our model. The experiment was recorded for only 10 minutes, but it has been reported that active holo-enzyme Rubisco takes about 25 minutes to become inactive and takes comparatively shorter time about 5 minutes to be actived from the inactive state (reviewed in section 1.5.1). The amount of RuBP in the process is also taken to be constant to reduce the modeling complexity. The enzyme Rubisco reacts with the sugar RuBP and forms enzyme complex E^{RuBP} (Eqn 2.1).

$$E + RuBP \xleftrightarrow{k_6, k_{-6}} E^{RuBP} \qquad (2.1)$$

Once enzyme complex E^{RuBP} has been formed it can either react with CO_2 or O_2, with probabilities depending on the surrounding CO_2 to O_2 ratio. The reaction of enzyme complex E^{RuBP} with CO_2 produces another complex $E^{RuBP}_{CO_2}$ (Eqn 2.2). The sub-complex $E^{RuBP}_{CO_2}$ breaks down into two molecules of 3-phosphoglycerate (3PG) and releases O_2 ultimately in photosynthesis (carboxylase reaction, eqn 2.3). It has been reported that several steps can be replaced by a delay term without affecting the dynamics.[56] The

release of O_2 in the photosynthesis process is represented as a delayed term, with delay τ_1 (Eqn 2.3). The term $O^{\tau_1}_{2(chl)}$ represents O_2 concentration in the chloroplast at τ_1 unit time after the breakdown of the $E^{RuBP}_{CO_2}$ complex.

$$E^{RuBP} + CO_{2\,(chl)} \xleftrightarrow{k_7,\, k_{-7}} E^{RuBP}_{CO_2} \tag{2.2}$$

$$E^{RuBP}_{CO_2} \xrightarrow{k_8} E + O^{\tau_1}_{2\,(chl)} \tag{2.3}$$

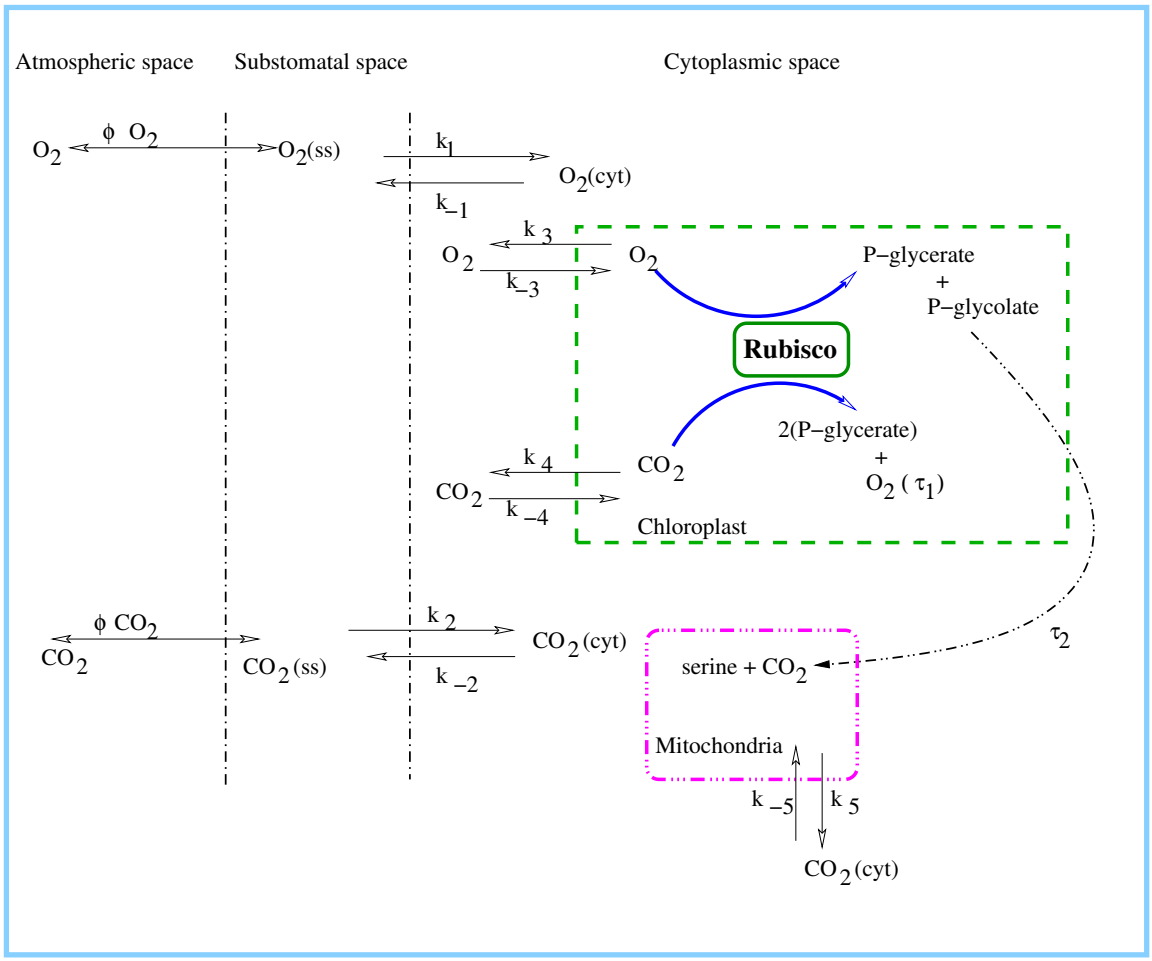

Figure 10: Illustration of the model, including diffusion of CO_2 and O_2 through different compartments, as well as the key chemical reactions.

The reaction of enzyme complex E^{RuBP} with O_2 produces another complex $E_{O_2}^{RuBP}$ (Eqn 2.4). The complex $E_{O_2}^{RuBP}$ turns into one molecule of 3PGA and one molecule of P-glycolate (oxygenase reaction, Eqn 2.5), but P-glycolate is toxic to plants and needs to be eliminated. Phosphoglycolate is converted into serine, which ultimately leads to the production of CO_2 in the mitochondria through a series of conversion steps (reviewed in section 1.6). In the model, we represent this series of conversions and transport steps by introducing another delay τ_2 (Eqn 2.5).

$$E^{RuBP} + O_{2\,(chl)} \xleftrightarrow{k_9,\, k_{-9}} E_{O_2}^{RuBP} \tag{2.4}$$

$$E_{O_2}^{RuBP} \xrightarrow{k_{10}} E + CO_{2\,(mito)}^{\tau_2} \tag{2.5}$$

Once CO_2 and O_2 is in the substomatal space, the next barrier to the diffusion is the plasma membrane and the organelle membrane. CO_2, O_2 and H_2O diffuse easily across the plasma membrane.[57] The organelle membranes such as mitochondrial and chloroplast membranes are the most rate-limiting to the diffusion of CO_2 and O_2. Both mitochondria and chloroplasts are highly involved with cellular metabolism and both have two membranes. The inner mitochondrial membrane forms mitochondrial cristae, in which all the enzymes (dehydrogenase and cytochromes) responsible for electron transfer are embedded. The space inside the inner membrane of the mitochondria is filled with viscous fluid known as the matrix, where all the enzymatic reactions take place. Of the two chloroplastic membranes, the outer one is more permeable to small solutes, just as for the mitochondrial outer membrane. Relatively high galactolipid and low protein contents are present in both chloroplastic membranes. The chlorophyll and other

photosynthetic pigments are attached with the protein present in the chloroplast membrane. The stroma, which is called the reaction center for photosynthesis and photorespiration since most of the reactions occur there, is the inside region of the inner chloroplastic membrane.[19, 48]

Once the CO_2 and O_2 overcome the barrier of the membrane, they can disperse throughout a compartment by diffusion as well as by cytoplasmic streaming.[19, 48] A correction factor, the partition coefficient, accounts for the concentration difference between compartments due to differences in chemical composition. The partition coefficient (K_{CO_2} or K_{O_2}) can be defined as the ratio of the concentration of CO_2 or O_2 in the two phases at equilibrium.[19, 48, 58] Hence, the partition coefficient is dimensionless. For example, the partition coefficient of CO_2 for substomatal space to cytoplasm at equilibrium is

$$K_{CO_2,\,ss/cyt} = \frac{\text{concentration of all forms of } CO_2 \text{ in substomatal space}}{\text{concentration of all forms of } CO_2 \text{ in cytoplasm}}$$

$$= \frac{C^{ss}_{CO_2}}{C^{cyt}_{CO_2} + C^{cyt}_{HCO_3^-} + C^{cyt}_{H_2CO_3}}$$

The partition coefficient indicates the accumulation efficiency of CO_2 in a particular compartment. For example, if the partition coefficient $K_{CO_2,\,cyt/chl}$ is larger than 1 then the CO_2 (CO_2 containing species) tends to accumulate in the cytoplasm rather than in the chloroplast. In contrast, if the partition coefficient $K_{CO_2,\,cyt/chl}$ is smaller than 1 then the CO_2 is accumulating in the chloroplast rather than in the cytoplasm.

2.3 Model equations

Model descriptions can be expressed mathematically into a set of differential equations. The equations are derived in the mass-action form generalized to include delays.[55] The diffusion of CO_2 and O_2 across compartments is considered as a flux. The flux is proportional to the corresponding concentration of gases. The unit of flux is mol/s. Before the formulation of differential equations, the flux has been calculated. As an example, the flux from the substomatal space to the cytoplasm has been described below.

2.3.1 Flux calculation

We expressed the net flux of CO_2 from the substomatal space to the cytoplasm of mesophyll tissue as

$$F_{\mathrm{CO_2\,(ss\rightarrow cyt)}} = k_2\left[\mathrm{CO_{2\,(ss)}}\right] - k_{-2}\left[\mathrm{CO_{2\,(cyt)}}\right].$$

At equilibrium, this flux would be zero, leading to the equation

$$\frac{\left[\mathrm{CO_{2\,(cyt)}}\right]}{\left[\mathrm{CO_{2\,(ss)}}\right]} = \frac{k_2}{k_{-2}} = K_{\mathrm{CO_2,\,cyt/ss}},$$

where $K_{\mathrm{CO_2,\,cyt/ss}}$ is the cytoplasm / substomatal partition coefficient.

Then the flux of CO_2 from the substomatal space to the cytoplasm of mesophyll tissue can be rewritten as

$$F_{\mathrm{CO_2\,(ss\rightarrow cyt)}} = k_2\left(\left[\mathrm{CO_{2\,(SS)}}\right] - \left[\mathrm{CO_{2\,(cyt)}}\right] / K_{\mathrm{CO_2,\,cyt/ss}}\right).$$

Similarly, the flux of CO_2 from the chloroplast to the cytoplasm of mesophyll tissue is

$$F_{\mathrm{CO_2\,(chl\rightarrow cyt)}} = k_4\left(\left[\mathrm{CO_{2\,(chl)}}\right] - \left[\mathrm{CO_{2\,(cyt)}}\right] / K_{\mathrm{CO_2,\,cyt/chl}}\right),$$

the flux of CO_2 from the mitochondria to the cytoplasm of mesophyll tissue is

$$F_{CO_2\,(mito\rightarrow cyt)} = k_5\left(\left[CO_{2\,(mito)}\right] - \left[CO_{2\,(cyt)}\right] / K_{CO_2,\,cyt/mito}\right),$$

the flux of O_2 from the sub-stomatal space to the cytoplasm of mesophyll tissue is

$$F_{O_2\,(ss\rightarrow cyt)} = k_2\left(\left[O_{2\,(ss)}\right] - \left[O_{2\,(cyt)}\right] / K_{O_2,\,cyt/ss}\right),$$

and the flux of O_2 from the chloroplast to the cytoplasm of mesophyll tissue is

$$F_{O_2\,(chl\rightarrow cyt)} = k_4\left(\left[O_{2\,(chl)}\right] - \left[O_{2\,(cyt)}\right] / K_{O_2,\,cyt/chl}\right).$$

The rate of change of concentration of CO_2 or O_2 in any compartment due to flux would be $F_{CO_2\text{ or }O_2}$ of corresponding compartments$/$volume of the particular compartment. For example, the rate of change of concentration of CO_2 in the cytoplasm due to flux would be $F_{CO_2(chl\rightarrow cyt)} / V_{(cyt)}$ and the rate of change of concentration of CO_2 in the chloroplast due to flux would be $-F_{CO_2(chl\rightarrow cyt)} / V_{(chl)}$.

2.3.2 Differential equations

The set of differential equations are as follows:

$$\frac{d}{dt}\left[E^{RuBP}\right] = k_6[RuBP]\left(E_t - \left[E^{RuBP}\right] - \left[E^{RuBP}_{CO_2}\right] - \left[E^{RuBP}_{O_2}\right]\right) - k_{-6}\left[E^{RuBP}\right] - k_7\left[E^{RuBP}\right]\left[CO_{2\,(chl)}\right]$$
$$+k_{-7}\left[E^{RuBP}_{CO_2}\right] + k_{-9}\left[E^{RuBP}_{O_2}\right] - k_9\left[E^{RuBP}\right]\left[O_{2\,(chl)}\right]$$

$$\frac{d}{dt}\left[E^{RuBP}_{CO_2}\right] = k_7\left[E^{RuBP}\right]\left[CO_{2\,(chl)}\right] - k_{-7}\left[E^{RuBP}_{CO_2}\right] - k_8\left[E^{RuBP}_{CO_2}\right]$$

$$\frac{d}{dt}\left[E^{RuBP}_{O_2}\right] = k_9\left[E^{RuBP}\right]\left[O_{2\,(chl)}\right] - k_{-9}\left[E^{RuBP}_{O_2}\right] - k_{-10}\left[E^{RuBP}_{O_2}\right]$$

$$\frac{d}{dt}\left[\mathrm{CO}_{2\,(\mathrm{cyt})}\right] = \left(F_{\mathrm{CO}_2\,(\mathrm{mito}\rightarrow\mathrm{cyt})} + F_{\mathrm{CO}_2\,(\mathrm{ss}\rightarrow\mathrm{cyt})} + F_{\mathrm{CO}_2\,(\mathrm{chl}\rightarrow\mathrm{cyt})}\right) \Big/ \mathrm{V}_{(\mathrm{cyt})}$$

$$\frac{d}{dt}\left[\mathrm{CO}_{2\,(\mathrm{ss})}\right] = \phi_{\mathrm{CO}_2}\left(\left[\mathrm{CO}_{2\,(\mathrm{atm})}\right] - \left[\mathrm{CO}_{2\,(\mathrm{ss})}\right]\right) - F_{\mathrm{CO}_2\,(\mathrm{ss}\rightarrow\mathrm{cyt})} \Big/ \mathrm{V}_{(\mathrm{ss})}$$

$$\frac{d}{dt}\left[\mathrm{CO}_{2\,(\mathrm{mito})}\right] = k_{10} \times \left[\mathrm{CO}^{\tau_2}_{2\,(\mathrm{mito})}\right] - F_{\mathrm{CO}_2\,(\mathrm{mito}\rightarrow\mathrm{cyt})} \Big/ \mathrm{V}_{(\mathrm{mito})}$$

$$\frac{d}{dt}\left[\mathrm{CO}_{2\,(\mathrm{chl})}\right] = k_{-7}\left[\mathrm{E}^{\mathrm{RuBP}}_{\mathrm{CO}_2}\right] - k_7\left[\mathrm{E}^{\mathrm{RuBP}}\right]\left[\mathrm{CO}_{2\,(\mathrm{chl})}\right] - F_{\mathrm{CO}_2\,(\mathrm{chl}\rightarrow\mathrm{cyt})} \Big/ \mathrm{V}_{(\mathrm{chl})}$$

$$\frac{d}{dt}\left[\mathrm{O}_{2\,(\mathrm{cyt})}\right] = \left(F_{\mathrm{O}_2\,(\mathrm{ss}\rightarrow\mathrm{cyt})} + F_{\mathrm{O}_2\,(\mathrm{chl}\rightarrow\mathrm{cyt})}\right) \Big/ \mathrm{V}_{(\mathrm{cyt})}$$

$$\frac{d}{dt}\left[\mathrm{O}_{2\,(\mathrm{ss})}\right] = \phi_{\mathrm{O}_2}\left(\left[\mathrm{O}_{2\,(\mathrm{atm})}\right] - \left[\mathrm{O}_{2\,(\mathrm{ss})}\right]\right) - F_{\mathrm{O}_2\,(\mathrm{ss}\rightarrow\mathrm{cyt})} \Big/ \mathrm{V}_{(\mathrm{ss})}$$

$$\frac{d}{dt}\left[\mathrm{O}_{2\,(\mathrm{chl})}\right] = k_{-9}\left[\mathrm{E}^{\mathrm{RuBP}}_{\mathrm{O}_2}\right] - k_9\left[\mathrm{E}^{\mathrm{RuBP}}\right]\left[\mathrm{O}_{2\,(\mathrm{chl})}\right] + k_8 \times \left[\mathrm{O}^{\tau_1}_{2\,(\mathrm{chl})}\right] - F_{\mathrm{O}_2\,(\mathrm{chl}\rightarrow\mathrm{cyt})} \Big/ \mathrm{V}_{(\mathrm{chl})}$$

2.3.3 Parameters

The parameters used in the model are presented below. Either parameters are taken from literature or calculated from data available in the literature, insofar as this was possible. In some cases best assumptions were made. First, the parameters are listed in table 2, and some calculations are shown later.

2.3.3.1 Calculations for Michaelis-Menten constants of Rubisco enzyme

The molecular weight and the specific activity of Rubisco are reported as 560 KDa [24] and 1.7 μmol (mg protein)$^{-1}$min^{-1} [59] respectively. The catalysis rate of carboxylation (k_{cat}) can be calculated as

$$k_{cat} = \text{Specific activity} \times \text{Molecular weight of Rubisco}$$
$$= \frac{1.7\ \mu\text{mol}}{\text{mg protein min}} \times \frac{10^{-6}\ \text{mol}}{1\ \mu\text{mol}} \times \frac{560{,}000\ \text{g}}{\text{mol}} \times \frac{1000\ \text{mg}}{\text{g}} \times \frac{1\ \text{min}}{60\ \text{s}}$$
$$= 16\ \text{s}^{-1}$$

Table 2: List of parameters used in the model.

Parameter	**Value**	**Comments**
$\mathbf{k_1}$	7 X 10^{-4} L s^{-1}	Calculated
$\mathbf{k_2}$	1.5 X 10^{-2}L s^{-1}	Calculated
$\mathbf{k_3}$	7 X 10^{-4} L s^{-1}	Estimated
$\mathbf{k_4}$	1.5 X 10^{-3} L s^{-1}	Brian et al., 1999[60]
$\mathbf{k_5}$	1.5 X 10^{-3}L s^{-1}	Brian et al., 1999[60]
$\mathbf{k_6}$	10^5 mM^{-1} s^{-1}	(Stroppolo et al., 2001[61])
$\mathbf{k_{-6}}$	270 s^{-1}	Calculated
$\mathbf{k_7}$	800 mM^{-1} s^{-1}	Calculated
$\mathbf{k_{-7}}$	1.6 s^{-1}	Calculated
$\mathbf{k_8}$	16 s^{-1}	Calculated
$\mathbf{k_9}$	25 mM^{-1} s^{-1}	Calculated
$\mathbf{k_{-9}}$	1.2 s^{-1}	Calculated
$\mathbf{k_{10}}$	12 s^{-1}	Calculated
ϕ_{CO_2}	1.84 s^{-1}	Hahn, 1987[62]
ϕ_{O_2}	2.24 s^{-1}	Estimated
τ_1	1 s	Estimated
τ_2	20-270 s	(Atkin et al., 2000[47])
$\mathbf{O_{2\ (atm)}}$	8.73 mM	Calculated
$\mathbf{CO_{2\ (atm)}}$	0.0015 mM	Calculated
RuBP	0.8 mM	Pickersgill, 1986[63]
$\mathbf{E_t}$	4 mM	Hitz and Stewart, 1980[64]
$K_{CO_2,\ cyt/chl}$	1	Estimated
$K_{CO_2,\ cyt/ss}$	0.017	Calculated
$K_{CO_2,\ cyt/mito}$	1	Estimated
$K_{O_2,\ cyt/ss}$	0.028	Calculated
$K_{O_2,\ cyt/chl}$	1	Estimated
$\mathbf{V_{(chl)}}$	890 X10^{-6} L	Winter et al.,1994[65]
$\mathbf{V_{(mito)}}$	28 X 10^{-6} L	Winter et al.,1994[65]
$\mathbf{V_{(cyt)}}$	186 X10^{-6} L	Winter et al.,1994[65]
$\mathbf{V_{(ss)}}$	1620 X10^{-6} L	Winter et al., 1994[65]

Total enzyme concentration (E_{total}) was reported as 4mM.[63, 66] The maximum velocity of the carboxylation ($v_{max\,(c)}$) reaction can be calculated as

$$v_{max(c)} = k_{cat} \times \text{Rubisco concentration}$$
$$= 16\ s^{-1} \times 4\text{mM}$$
$$= 64\ \text{mM}\ s^{-1}$$

We have, according to Von Caemmerer et al., 1994 [67]

$$\frac{v_{max(o)}}{v_{max(c)}} = 0.77$$
$$\Rightarrow v_{max(o)} = v_{max(c)} \times 0.77 = 64\ \text{mM}\ s^{-1} \times 0.77$$
$$\Rightarrow v_{max(o)} = 49\ \text{mM}\ s^{-1}$$

We can get the k_{10} as

$$k_{10} = \frac{v_{max(o)}}{E_{total}} = \frac{49\ \text{mM}\ s^{-1}}{4\ \text{mM}} = 12\ s^{-1}.$$

Assuming $k_{cat} = k_8$, we get $k_8 = 16\ s^{-1}$.

Since it is known that once CO_2 binds with the enzyme complex the reaction rarely goes in the reverse direction, [68] k_{-7} is likely to be small. We approximated it as 10% of k_8, so

$k_{-7} = 1.6\ s^{-1}$.

Similarly, k_{-9} could be approximated as 10% of k_{10}, so

$k_{-9} = 1.2\ s^{-1}$.

The K_m of the carboxylation reaction is $22\ \mu\text{M}$.[69] Using this Michaelis-Menten constant, we get k_7 as

$$k_7 = \frac{k_{-7} + k_8}{K_{m\,(c)}} = \frac{(1.6 + 16)s^{-1}}{22\ \mu\text{M} \times 10^{-3}\text{mM}/\mu\text{M}} = 800\ \text{mM}^{-1}\ s^{-1}.$$

The K_m of the oxygenation reaction is 532 μM.[69] Similarly, we can get k_9 as

$$k_9 = \frac{k_{-9} + k_{10}}{K_{m(o)}} = \frac{(1.2+12)\ s^{-1}}{532\ \mu M \times 10^{-3} mM/\mu M} = 25\ mM^{-1}\ s^{-1}$$

The K_m of the E^{RuBP} complex is about [70] 2.7 μM, and according to Stroppolo et al., 2001,[61] $k_6 = 10^8\ M^{-1}\ s^{-1} = 10^5 mM^{-1}s^{-1}$. We can get k_{-6} as

$$K_m = \frac{k_{-6}}{k_6}$$
$$\Rightarrow k_{-6} = K_m \times k_6$$
$$\Rightarrow k_{-6} = (2.7 \times 10^{-3})\ mM \times 10^5 mM^{-1}s^{-1}$$
$$\Rightarrow k_{-6} = 2.7 \times 10^2\ s^{-1}$$

2.3.3.2 Calculations for different compartmental volume

According to Lawlor, 2001[71] the volume per unit area of a C_3 plant leaf is $3 \times 10^{-4}\ m^3/m^2$ and a typical tobacco leaf area is $A_{(leaf)} = (20 \times 10)\ cm^2 = 0.02\ m^2$. So, we can get the typical tobacco leaf volume as

$$V_{(leaf)} = \left(3 \times 10^{-4} \times 0.02\right) m^3 = 6 \times 10^{-6}\ m^3 \times \frac{1000\ L}{1\ m^3} = 6 \times 10^{-3}\ L$$

According to Winter et al., 1994[65] the cytoplasmic volume is 24 μL (mg chl)$^{-1}$ and the chlorophyll content is 1.29 mg chl g^{-1}. The density of cytoplasm is assumed to be 1 g/mL. Thus the cytoplasmic volume can be represented as

$$V_{(cyt)} = 24\ \mu L\ (\text{mg chl})^{-1}$$
$$= \frac{24\ \mu L}{\text{mg chl}} \times \frac{1.29\ \text{mg chl}}{\text{g}} \times \frac{1\ \text{g}}{1\ \text{mL}} \times V_{(leaf)}$$
$$= \frac{30.96\ \mu L}{\text{mL}} \times \frac{1\ \text{mL}}{1000\ \mu L} \times \left(6 \times 10^{-3}\right) \text{L}$$
$$= 186 \times 10^{-6}\ \text{L}$$

Again according to Winter et al., 1994,[65] the mitochondrial volume is 3.6 μL (mg chl)$^{-1}$. Thus the volume can be represented as

$$V_{(mito)} = 3.6\ \mu L\ (\text{mg chl})^{-1}$$
$$= \frac{3.6\ \mu L}{\text{mg chl}} \times \frac{1.29\ \text{mg chl}}{\text{g}} \times \frac{1\ \text{g}}{1\ \text{mL}} \times V_{(leaf)}$$
$$= \frac{4.644\ \mu L}{\text{mL}} \times \frac{1\ \text{mL}}{1000\ \mu L} \times \left(6 \times 10^{-3}\right) \text{L}$$
$$= 28 \times 10^{-6}\ \text{L}$$

According to Winter et al., 1994,[65] the chloroplastic volume is 115 μL (mg chl)$^{-1}$. Thus the volume can be shown as

$$V_{(chl)} = 115\ \mu L\ (\text{mg chl})^{-1}$$
$$= \frac{115\ \mu L}{\text{mg chl}} \times \frac{1.29\ \text{mg chl}}{\text{g}} \times \frac{1\ \text{g}}{1\ \text{mL}} \times V_{(leaf)}$$
$$= \frac{148.350\ \mu L}{\text{mL}} \times \frac{1\ \text{mL}}{1000\ \mu L} \times \left(6 \times 10^{-3}\right) \text{L}$$
$$= 890 \times 10^{-6}\ \text{L}$$

According to Lawlor, 2001,[71] the substomatal volume is 27% of total leaf volume. Thus the volume can be represented as

$$V_{(SS)} = 0.27\ V_{(leaf)}$$
$$= 0.27 \times \left(6 \times 10^{-3}\right) \text{ L}$$
$$= \ 1.6 \times 10^{-3} \text{ L}$$

2.3.3.3 Calculation for permeability coefficient

The permeability coefficient for CO_2 from substomatal space to cytoplasm is about 9 x 10^{-3} cm/s.[72] The radius of mesophyll cell in a C_3 plant is 1.5 X 10^{-5} m.[71] We can get the surface area of a (spherical) cell,

$$A = 4\ \pi r^2 = 4 \times \pi \times \left(1.5 \times 10^{-5}\right)^2 = 2.8 \times 10^{-9} m^2$$

The total number of spongy mesophyll cells is about 3 x 10^9 cells/m^2 in a C_3 plant leaf. We can get the total number of spongy mesophyll cells in typical tobacco leaf area,

$$\text{Number of cells} = 3 \times 10^9 \times 0.02 = \ 6 \times 10^7.$$

We get,

$$\text{Total area of spongy mesophyll cells} = \ 2.8 \times 10^{-9}\ m^2 \times 6 \times 10^7$$
$$= 0.168\ m^2 = 1680\ cm^2,$$

The permeability coefficient for CO_2 in between the substomatal space and cytoplasm is

$$k_2 = 9\times10^{-3}\,\frac{\text{cm}}{\text{s}}\times 1680\ \text{cm}^2$$
$$=15.12\,\frac{\text{cm}^3}{\text{s}}$$
$$=15.12\,\frac{\text{mL}}{\text{s}}$$
$$=0.015\ \text{L s}^{-1}$$

According to Gorton et al., 2003, [73] the permeability of CO_2 is 21 times larger relative to O_2, so we can get

$k_1 = 0.015/21 = 7\times10^{-4}\ \text{L s}^{-1}$.

Similarly, we can get $k_3 = 7\times10^{-4}\ \text{L s}^{-1}$.

The permeability coefficient for CO_2 in mitochondria is about[60] 2000 μmol min^{-1} (mg chl)$^{-1}$ mM^{-1} and the fresh weight of C_3 leaf[71] = 0.17 g/m^2. The permeability coefficient for CO_2 in mitochondria can be calculated as

$$\text{k}_4 = \frac{2000\ \mu\text{mol}}{\text{min (mg chl) mM}}$$
$$=\frac{0.002\text{mol}}{\text{min (mg chl)}}\times\frac{\text{L}}{\text{mmol}}\times\frac{1000\ \text{mmol}}{1\text{mol}}$$
$$=\frac{2\ \text{L}}{\text{min (mg chl)}}\times\frac{1.29\ \text{mg chl}}{1\text{g}}\times(0.17\,\frac{\text{g}}{\text{m}^2}\times 0.02\ \text{m}^2)\ \text{g}\times\frac{1\text{min}}{60\ \text{s}}$$
$$=1.5\times10^{-3}\ \text{L s}^{-1}$$

The permeability coefficient for CO_2 the chloroplast is assumed to be the same as the chemical composition for the compartments are similar. So, $k_5 = 1.5\times10^{-3}\ \text{L s}^{-1}$. [71]

2.3.3.4 Calculation of partition coefficients

The partition coefficients $K_{CO_2,\,cyt/ss}$ and $K_{O_2,\,cyt/ss}$ can be calculated according to Henry's Law. The Henry's law constant (K_H) for CO_2 and O_2 in water is 1.5 x 10^8 Pa/M and 7.92 x 10^7 Pa/M, respectively.[74]

We get,

$$K_H = \frac{P_{CO_2\,(ss)}}{\left[CO_{2\,(cyt)}\right]} = 1.5 \times 10^8 \text{ Pa/M},$$

According to the ideal gas law we get,

$$\frac{n}{V} = \frac{P}{RT} = \frac{1.5 \times 10^8 \text{ Pa}}{8.314 \frac{\text{J}}{\text{mol K}} \times 298 \text{ K}} = \frac{1.5 \times 10^8 \text{ Pa}}{2478 \frac{\text{Pa m}^3}{\text{mol K}} \times \frac{1000 \text{ L}}{\text{m}^3}} = 60.5 \text{ mol/L}$$

where the gas constant R= 8.314 J/mol K and the temperature is 25^0 C.

So,

$$K_H \equiv 60.5.$$

In our model, we defined the partition constant of CO_2 from the cytoplasm to substomatal space ($K_{CO_2,\,cyt \rightarrow ss}$). So, we can get $K_{CO_2,\,cyt/ss}$ value if we inverse the K_H value.

The partition coefficient is therefore

$$K_{CO_2,\,cyt/ss} = \frac{1}{60.5} = 0.017$$

Similarly, we can get the partition coefficient for O_2 gas,

$$K_{O_2,\,cyt/ss} = 0.028$$

2.3.3.5 Calculation for converting µl L^{-1} (ppm) into mM

I need to convert the experimental CO_2 concentration unit (µl L^{-1}) into mM in my model for consistency in the units. Standard atmospheric pressure is 101325 Pa (P_{total}). In the experiment, the plants were transferred from the atmospheric CO_2 concentration (about 360 µl L^{-1}) to low CO_2 concentration (36 µl L^{-1}). Under normal atmospheric conditions, we get the partial pressure of CO_2,

$$P_{CO_2} = 101325 \times 360 \times 10^{-6} = 36.5 \text{ Pa}$$

According to the ideal gas law we get,

$$\frac{n}{V} = \frac{P_{CO_2}}{RT} = \frac{36.5 \text{ Pa}}{8.314 \frac{J}{\text{mol K}} \times 298\text{K}} = 0.015 \ \frac{\text{mol}}{\text{m}^3} \times \frac{\text{m}^3}{1000 \text{ L}} \times 1000 \ \frac{\text{mmol}}{\text{mol}} = 0.015 \text{ mM}.$$

Chapter 3: Mathematical analysis

3.1 Introduction

The mathematical analysis was performed to verify whether oscillations are possible following a theorem[75, 76] that was developed in our lab. Several biochemical systems have been analyzed through the theorem to assess the capability of the respective system to oscillate.[75, 76] In this chapter, we will discuss the mathematical analysis through which we will find out if our model has the potential to oscillate or not.

Using mass-action kinetics, a set of ordinary differential equations (ODEs) of a biochemical system has been derived which rule the time evolution of the concentrations. Once a model of a biochemical system has been developed, it is useful to determine whether the model can replicate any particular experimentally observed qualitative behavior like oscillations. This type of qualitative analysis of a biochemical model through mathematical analysis was started in the 1970s.[77, 78, 79] Graph-theoretical methods are an important tool to assist in this type of qualitative analysis.[75, 76] Stoichiometric Network Analysis (SNA) was the basis for developing the theorem.[75, 76] SNA theory was developed by Clarke[77, 78, 79] and some improvement were made by Ivanova.[80]

The analysis of models with delays (generated by delay-differential equations, DDEs) and without delays (generated by ODEs) is different. Our model is a DDE model. DDE models are common in the description of genetic regulation, particularly to avoid treating transcription and translation in detail. DDE models may represent other biochemical

systems where product appearance can be represented by delays such as in our model.

3.2 Bipartite graph, fragment and subgraph

Usually a graph is a set of vertices (a corner where two or more edges meet) that are connected by edges (or arcs; a line or link connecting a pair of vertices). The bipartite graph consists of a triple $G=(U,V,E)$ where U and V are two disjoint sets of vertices and E is the set of edges. In a biochemical system, the reactants and products could be the set U, where $U=\{A_1,A_2,A_3,.....,A_n\}$, and all the reactions could be the set V where $V=\{R_1,R_2,R_3,.....,R_m\}$ (fig 11). In fig 11, an edge (e_1) was drawn from A_1 to R_2, meaning that A_1 is a reactant in reaction 2. Similarly, another edge (e_2) was drawn from R_2 to A_3, indicating that A_3 is a product in reaction 2. Therefore the set of edges is $E(e_1,e_2.....)$ and thus $G=\{U,V,E\}$ is the bipartite graph of the system (fig 11).

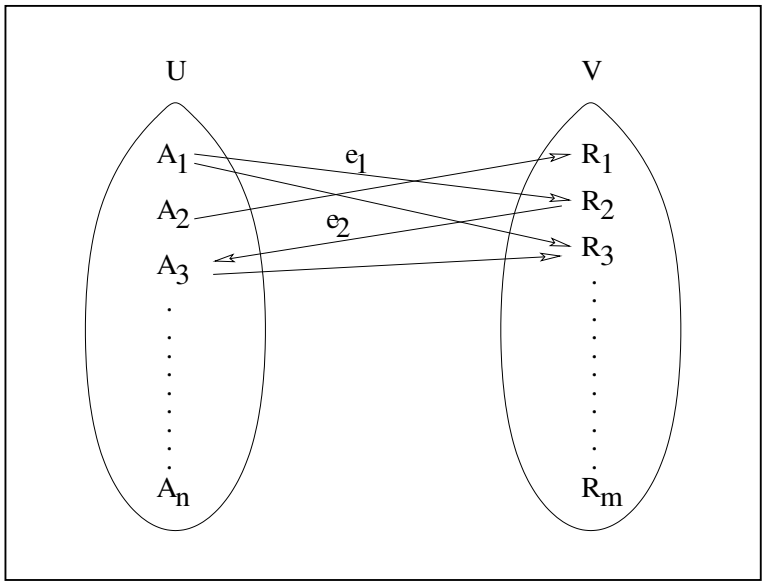

Figure 11: The bipartite graph

A sequence of vertices $\{A_i, R_j, A_k\}$ is called a path if the edges (A_i, R_j) and (R_j, A_k) belong to E. In fig 11, $\{A_1, R_2, A_3\}$ is described as a path as the edges (A_1, R_2) and (R_2, A_3) belong to E. One important note in here is that the paths have to start at a reactant and not a product. The edges (A_1, R_2) and (R_2, A_3) form a positive path [A_1, R_2, A_3] where A_1 and A_3 are the reactant and product respectively in reaction 2 (fig 11). Similarly, the edges (A_1, R_3) and (R_3, A_3) form negative paths $\overline{[A_1, R_3, A_3]}$ and $\overline{[A_3, R_3, A_1]}$ where A_1 and A_3 are the reactants in the reaction 3 (fig 11). A collection of paths can be called a cycle if the last vertex (element) of a path (from the U set) is the first vertex (element) in the next path all the way around, with the last element of the last path being the first element of the first path. A cycle is positive if it contains an even number of negative paths or all paths are positive (fig 12 C_1 and C_2). Similarly a cycle is negative if it contains an odd number of negative paths. The paths $[A_1, R_2, A_3]$ and $[A_3, R_3, A_1]$ form a positive cycle as both paths are positive paths (fig 13 C_1). And the negative $\overline{[A_1, R_3, A_3]}$ paths and $\overline{[A_3, R_3, A_1]}$ form a positive cycle (though it does not look like cycle) as it contains two negative paths (fig 12 C_2). The paths $[A_1, R_2, A_3]$ and $\overline{[A_3, R_3, A_1]}$ form a negative cycle (fig 12 C_3) as it has one negative path. A subgraph (g) is a set of cycles or edges, $g = \{C_1, C_2, C_3 ..... C_s\}$ where each C_i can be either an edge with its associated pair of vertices, or a cycle, and the opening vertex of every edge or path is from the set U. The number of vertices of a subgraph (i.e number of chemical species in a subgraph) determines the order of the subgraph (g_1, g_2,……g_y, where the

subscripts are the number of vertices). The set of subgraphs of order k with the same U and V sets is called a fragment, denoted by S_k. For example, if the subgraphs (g_1, g_2 …..) belong the same fragment and if the number of vertices in set U (number of reactants and products) and in set V (number of reactions) are 6, then we denote the fragment by S_6.

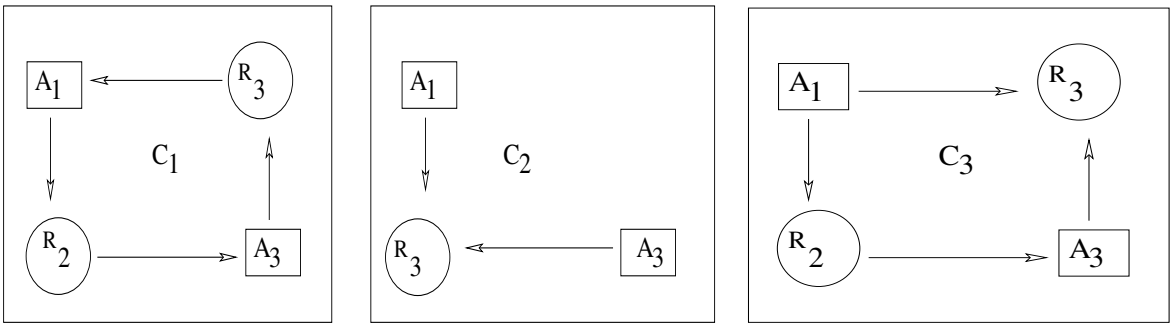

Figure 12: The cycles: positive (C1 and C2) and negative cycles (C3) are shown here.

3.2.1 Theorem for ODE

The method of analysis is different for ODE and DDE models. In this section, the theorem for an ODE model will be discussed. According to the theorem[75, 76] if {g} is the set of subgraphs of bipartite graph G of order n and t_g is the number of cycles in each subgraph then

$$\det(-J) = \sum_{g \in G} K_g, \qquad (3.1)$$

where K_g is a product over all cycles and edges of subgraph g:

$$K_g = (-1)^{t_g} \prod_{[A_k, B_j] \in g} \alpha_{jk}^2 \sum_{C \in g} K_C, \qquad (3.2)$$

where α_{jk} is the stoichiometric coefficient for reactant k in reaction j, and K_C is a product over all positive and negative paths of a cycle:

$$K_C = \prod_{[\overline{A_k},B_j,\overline{A_i}] \in C} (-\alpha_{jk}\alpha_{ji}) \prod_{[A_k,B_j,A_i] \in C} (\alpha_{jk}\beta_{ji}), \qquad (3.3)$$

where β_{ji} is the stoichiometric coefficient for product i in reaction j.

We define, for a fragment S_k,

$$K_{S_k} = \sum_{g \in S_k \binom{i_1 \ldots\ldots i_k}{j_1 \ldots\ldots j_k}} K_g \qquad (3.4)$$

If $K_{S_k} < 0$ then the fragment can be called critical to produce oscillations. A critical fragment is a necessary (but not sufficient) condition for oscillations.

3.2.2 Theorem for DDE

The bipartite graph is the same for the ODE and DDE models. The calculation of K_{S_k} is almost similar for ODEs and DDEs following the equations described above, except eqn. 3.3. According to a theorem,[76] for a DDE model, eqn 3.3 is replaced by

$$K_C = \prod_{[\overline{A_k},B_j,\overline{A_i}] \in C} (\alpha_{jk}\alpha_{ji}) \prod_{[A_k,B_j,A_i] \in C} (\alpha_{jk}\beta_{ji}). \qquad (3.5)$$

3.3 Graph theory in our model

The delay-induced oscillations theorem[76] has been followed in our mathematical analysis. Bifurcation theory is the mathematical study of the qualitative changes of the dynamical behavior of a system. A change in a parameter causes a change in the stability of an attractor in a local bifurcation, e.g. a steady state becomes unstable and an oscillatory attractor appears in a Hopf bifurcation. SNA theory can describe the bifurcation potential of a chemical system depending on the reaction network. In the ODE model, bifurcation occurs only when one of the coefficients of the characteristic polynomial of the

Jacobian matrix changes sign. This means that the coefficient should have at least one negative term in it; the subgraph that has the negative terms could potentially be a subnetwork responsible for oscillations. More precisely for the delay-induced ODE model, the presence of a subgraph of the bipartite graph with a negative cycle is the necessary condition for oscillations.

For the mathematical analysis, first we need to build a bipartite graph. For this purpose, all the elementary reactions (from fig 10 in chapter 2 and eqn 2.1-2.5) from the model have been taken into consideration. We built a bipartite graph (fig 13) where the vertices are shown as circles or rectangular boxes and the vertices are connected by directed edges. The circle vertices are either reactants or products. The circle is a reactant if a directed edge starts from that circle and a product if a directed edge ends there. The rectangular boxes represents reactions. The reaction numbering (R) follows the numbering of the corresponding rate constants. For example, oxygen is entering from the substomatal place to the chloroplastic space with rate constant k_1, and with rate constant k_{-1} for the reverse process. In the bipartite graph these reverse reactions are shown as R_1 and R_{-1}, respectively.

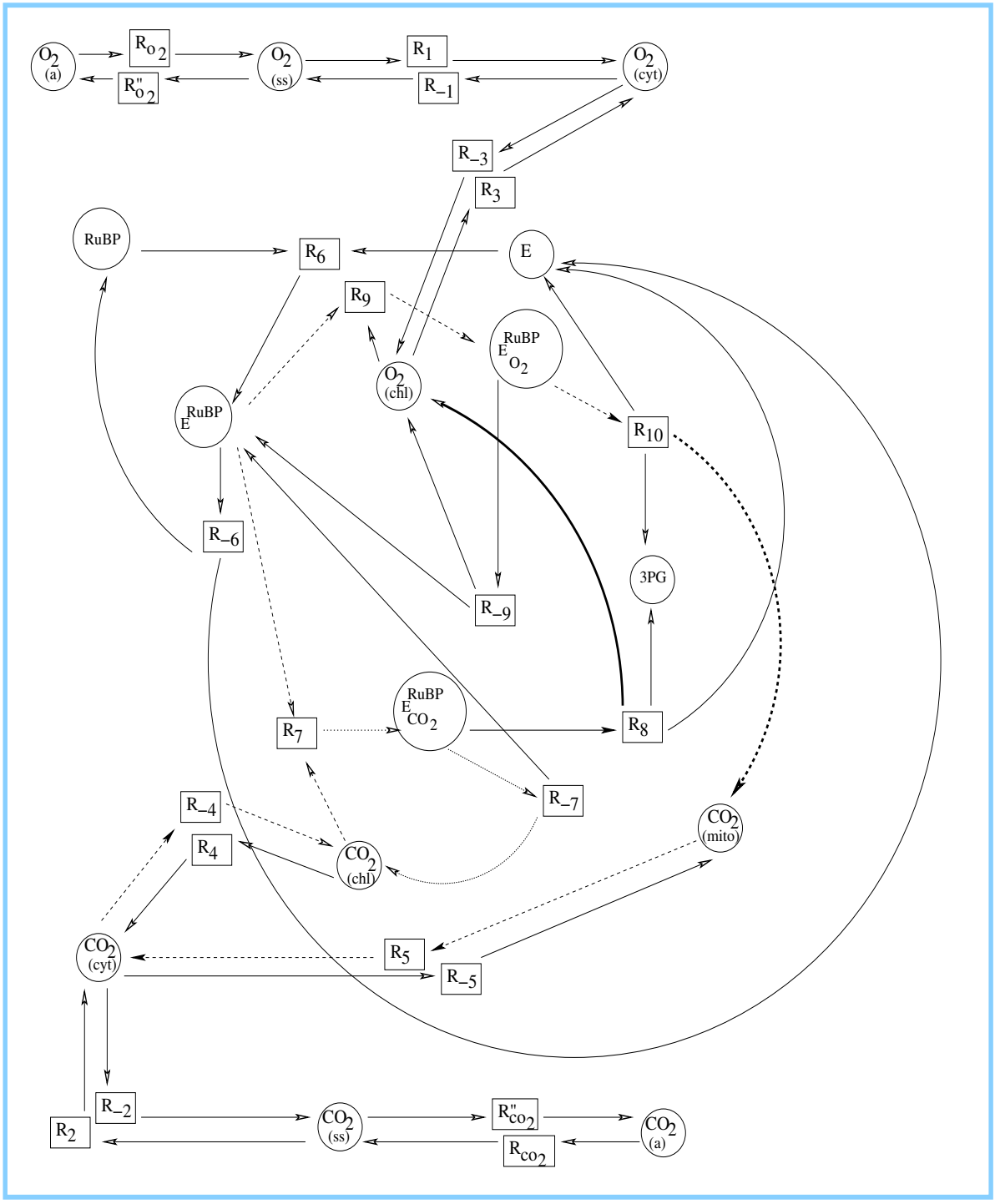

Figure 13: The bipartite graph corresponding to the reactions and transport of CO_2 and O_2 across the plant leaf. Dotted lines represent the small cycle and dashed lines represent the large cycle in the critical fragment. The delay terms are represented by bold lines.

3.4 Calculation of K_{S_k} in the DDE model

As mentioned earlier, the ODE and DDE models share the same bipartite graph. The necessary condition for delay-induced instability is the presence of at least one critical fragment in $\hat{G}$, the isomorphic bipartite graph to G, which includes at least one of the delayed reactions and which is not a critical fragment in the ODE model (that is shown in next section). In this model, we found the fragment of order six, $\mathrm{S}_6 = \begin{pmatrix} \mathrm{E}^{\mathrm{RuBP}} & \mathrm{E}_{\mathrm{O}_2}^{\mathrm{RuBP}} & \mathrm{CO}_{2\,(\mathrm{mito})} & \mathrm{CO}_{2\,(\mathrm{cyt})} & \mathrm{CO}_{2\,(\mathrm{chl})} & \mathrm{E}_{\mathrm{CO}_2}^{\mathrm{RuBP}} \\ \mathrm{R}_9 & \mathrm{R}_{10} & \mathrm{R}_5 & \mathrm{R}_{-4} & \mathrm{R}_7 & \mathrm{R}_{-7} \end{pmatrix}$. The fragment $S_6 \in \mathrm{G}$ contains three subgraphs (fig 14) as follows:

$$g_1 = \left\{ \left[E^{RuBP}, R_9 \right], \left[E_{O_2}^{RuBP}, R_{10} \right], \left[CO_{2(mito)}, R_5 \right], \left[CO_{2(cyt)}, R_{-4} \right], \left[CO_{2(chl)}, R_7 \right], \left[E_{CO_2}^{RuBP}, R_{-7} \right] \right\}$$

$$g_2 = \left\{ \left[E^{RuBP}, R_9 \right], \left[E_{O_2}^{RuBP}, R_{10} \right], \left[CO_{2(mito)}, R_5 \right], \left[CO_{2(cyt)}, R_{-4} \right], \mathrm{C} \begin{pmatrix} E_{CO_2}^{RuBP}, & CO_{2\,(chl)} \\ R_{-7}, & R_7 \end{pmatrix} \right\}$$

$$\mathrm{g}_3 = \left\{ \left[\mathrm{E}_{\mathrm{CO}_2}^{\mathrm{RuBP}}, \mathrm{R}_{-7} \right], \mathrm{C} \begin{pmatrix} \mathrm{E}^{\mathrm{RuBP}} & \mathrm{E}_{\mathrm{O}_2}^{\mathrm{RuBP}} & \mathrm{CO}_{2\,(\mathrm{mito})} & \mathrm{CO}_{2\,(\mathrm{cyt})} & \mathrm{CO}_{2\,(\mathrm{chl})} \\ \mathrm{R}_9 & \mathrm{R}_{10} & \mathrm{R}_5 & \mathrm{R}_{-4} & \mathrm{R}_7 \end{pmatrix} \right\}$$

The small cycle in g_2 is positive and the large cycle in g_3 is negative and contains one of the delayed reactions of the model. The calculation of the subgraph characteristics is as follows:

$K_{g_1} = (-1)^0 (1)$
$= 1$

$\mathrm{t_g} = 0$ and the product over cycles $\prod_{C \in g} K_C$ is also neglected as the subgraph has no cycle in it.

$$K_{g_2} = (-1)^1 (1) \prod_{C \in g} K_C$$

$K_C = (1)(1) = 1$ According to eqn 3.5, both for positive and negative paths in a cycle, the product of coefficients is 1.

Now,

$$K_{g_2} = (-1)^1(1)\prod_{C\in g} K_C = (-1)(1)(1) = -1.$$

and

$$K_{g_3} = (-1)^1(1)\prod_{C\in g} K_C = (-1)(1)(1) = -1.$$

The value of $\hat{K}_{S_6}$ can be calculated:

$$\hat{K}_{S_6} = \sum_{g\in S_6} K_g = K_{g_1} + K_{g_2} + K_{g_3} = 1-1-1 = -1 < 0,$$

making the fragment critical.

3.5 Calculation of K_{S_k} in the ODE model

We mentioned earlier that the bipartite graph for the ODE and DDE models are the same. The bipartite graph therefore decomposes into the same fragments and the subgraphs are the same in both cases. The calculation of K_{S_k} in the ODE model is shown below. According to eqn 3.5 the K_C value will be different compared to DDE models for subgraph g_3 as follows:

$K_C = (-1)(1) = -1$ For the negative path $\left[\overline{\mathrm{E}^{\mathrm{RuBP}}, \mathrm{R}_{-7}, \mathrm{CO}_{2\,(\mathrm{chl})}}\right]$ the product of coefficients will be -1 and for all other positive path the value will be 1.

And the ultimate g_3 value will be,

$$K_{g_3} = (-1)^1(1)\prod_{C\in g} K_C = (-1)(1)(-1) = 1.$$

So, the fragment produces the following characteristic value:

$\hat{K}_{S_6} = \sum_{g \in S_6} K_g = K_{g_1} + K_{g_2} + K_{g_3} = 1 - 1 + 1 = 1 > 0$, confirming that $S_6 \in G$ is not critical.

An attempt was made to search for other critical fragments in the ODE model and none were found. Therefore, oscillations are not possible in the ODE model. At this point, it is easy to conclude that without a delay (in eqn 2.5), it is impossible to produce oscillations. Any oscillations observed therefore belong to the class of delay-induced oscillations.

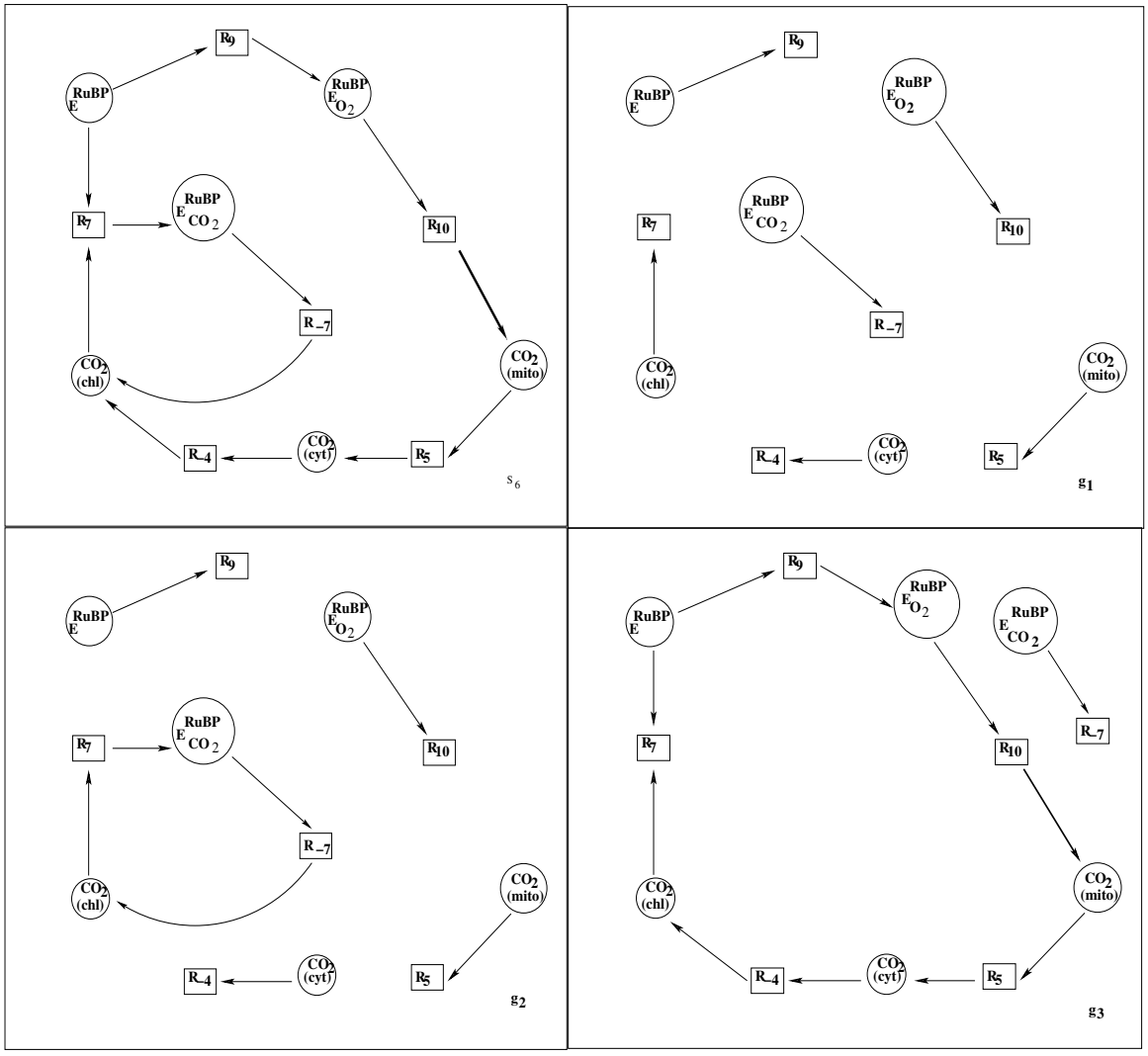

Figure 14: The fragments of order six (S_6) and the subgraphs (g_1, g_2, g_3) for the carboxylase reaction are shown in the figure.

Chapter 4: Computational analysis

4.1 Introduction

In this chapter I will discuss the results derived through computer simulations. The model and the parameter set described in the previous chapter were used for the computer simulations. The software XPPaut was used for the simulations.[81] In producing the oscillations, I tried to keep our parameter values in the physiological range. Carboxylase and oxygenase reaction kinetics are crucial to produce oscillations. The oxygenase reaction kinetics (e.g. catalytic rate constant and K_m ratio) are straightforward to maintain in the physiological range but it was very difficult for the carboxylase reaction kinetics while producing oscillations.

4.2 Regular and irregular oscillations

The model produces irregular oscillations (fig 15) in the parameter set 1. These irregular oscillations are most likely chaotic transient oscillations. These transient chaotic oscillations transform into regular oscillations eventually. The period of oscillations in this regime is proportional to the delay τ_2. The system is oscillating within the range of 80-110 ppm of substomatal CO_2 (fig 15 a) which does not agree with the experimental observation in terms of the oscillation range, where the system was oscillating within 34-38 ppm of internal CO_2 roughly every few seconds. From fig 15 b, it is clear that the system is oscillating within the range of 700-1200 ppm of chloroplastic CO_2 every 25 s.

This range and the period of the irregular oscillations is not compatible with the experimental observations.

Table 3: Three parameter sets used in this thesis.

Parameters	**Parameter set 1**	**Parameter set 2**	**Parameter set 3**
$\mathbf{k_1}$	0.01 L s^{-1}	7 X 10^{-4} L s^{-1}	7 X 10^{-4} L s^{-1}
$\mathbf{k_2}$	0.01 L s^{-1}	1.5 X 10^{-2} L s^{-1}	1.5 X 10^{-2} L s^{-1}
$\mathbf{k_3}$	1 L s^{-1}	7 X 10^{-4} L s^{-1}	7 X 10^{-3} L s^{-1}
$\mathbf{k_4}$	1.5 X 10^{-3} L s^{-1}	1.5 X 10^{-2} L s^{-1}	1.5 X 10^{-3} L s^{-1}
$\mathbf{k_5}$	0.15 L s^{-1}	1.5 X 10^{-2} L s^{-1}	1.5 X 10^{-3} L s^{-1}
$\mathbf{k_6}$	10^5 mM^{-1} s^{-1}	10^5 mM^{-1} s^{-1}	10^5 mM^{-1} s^{-1}
$\mathbf{k_{-6}}$	270 s^{-1}	270 s^{-1}	270 s^{-1}
$\mathbf{k_7}$	60 mM^{-1} s^{-1}	400 mM^{-1} s^{-1}	2.5 mM^{-1} s^{-1}
$\mathbf{k_{-7}}$	.0016 s^{-1}	0.0001 s^{-1}	0.00001 s^{-1}
$\mathbf{k_8}$	0.003 s^{-1}	0.016 s^{-1}	0.0025 s^{-1}
$\mathbf{k_9}$	250 mM^{-1} s^{-1}	250 mM^{-1} s^{-1}	250 mM^{-1} s^{-1}
$\mathbf{k_{-9}}$	120 s^{-1}	100 s^{-1}	120 s^{-1}
$\mathbf{k_{10}}$	120 s^{-1}	10 s^{-1}	12 s^{-1}
ϕ_{CO_2}	1.84 s^{-1}	1.8 s^{-1}	.02 s^{-1}
ϕ_{O_2}	0.0453 s^{-1}	2.25 s^{-1}	.025 s^{-1}
τ_1	1 s	1 s	1 s
τ_2	40 s	20 s	270 s
$\mathbf{O_{2\ (atm)}}$	8.73 mM	8.73 mM	8.73 mM
$\mathbf{CO_{2\ (atm)}}$	0.0015 mM	0.0015 mM	0.0015 mM
RuBP	1.6 mM	0.8 mM	0.8 mM
$\mathbf{E_t}$	4 mM	4 mM	3.5 mM
$K_{CO_2,\,cyt/chl}$	0.1	0.5	0.1
$K_{CO_2,\,cyt/ss}$	1	1	30
$K_{CO_2,\,cyt/mito}$	0.5	0.01	0.1
$K_{O_2,\,cyt/ss}$	10	10	0.5
$K_{O_2,\,cyt/chl}$	10	10	15
$\mathbf{V_{(chl)}}$	890 X10^{-6} L	890 X10^{-6} L	890 X10^{-6} L
$\mathbf{V_{(mito)}}$	28 X 10^{-6} L	28 X 10^{-6} L	28 X 10^{-6} L
$\mathbf{V_{(cyt)}}$	186 X10^{-6} L	186 X10^{-6} L	186 X10^{-6} L
$\mathbf{V_{(ss)}}$	1620 X10^{-6} L	1620 X10^{-6} L	1620 X10^{-6} L

The chloroplastic CO_2 in an experiment[20] is calculated as about 280 ppm at ambient atmospheric condition. In contrast, the irregular oscillations are produced in my simulation at low CO_2 concentration (about 36 ppm). Hence, the high substomatal and chloroplastic concentration of CO_2 can be explained in terms of the unrealistic parameter set 1 (table 3) used in my simulation. In particular, the model is generating unreasonably high CO_2 concentration in different compartments at the parameter set 1.

We call a parameter set "non-physiological" if some of the parameter values in that set are far from the physiological range (Table 2). In contrast, a parameter set is referred to as "physiological" if the parameters are close to the physiological range. The parameter set 1 that supports the transient chaotic oscillations is a non-physiological parameter set. In particular, the K_m ratio of carboxylase is $5x10^{-5}$ mM, and the catalytic rate constants of the oxygenase and carboxylase reactions (0.003 s^{-1} and 120 s^{-1} respectively) are in a non-physiological range (Table 3). Furthermore, the period and the oscillating range are slower and higher (fig 15), respectively, compared to the experimentally observed oscillations.[8] The transient oscillations produced in our model do not match up with the experimental observations[8] but do show that this type of irregular oscillations is possible in this model for a certain set of parameters.

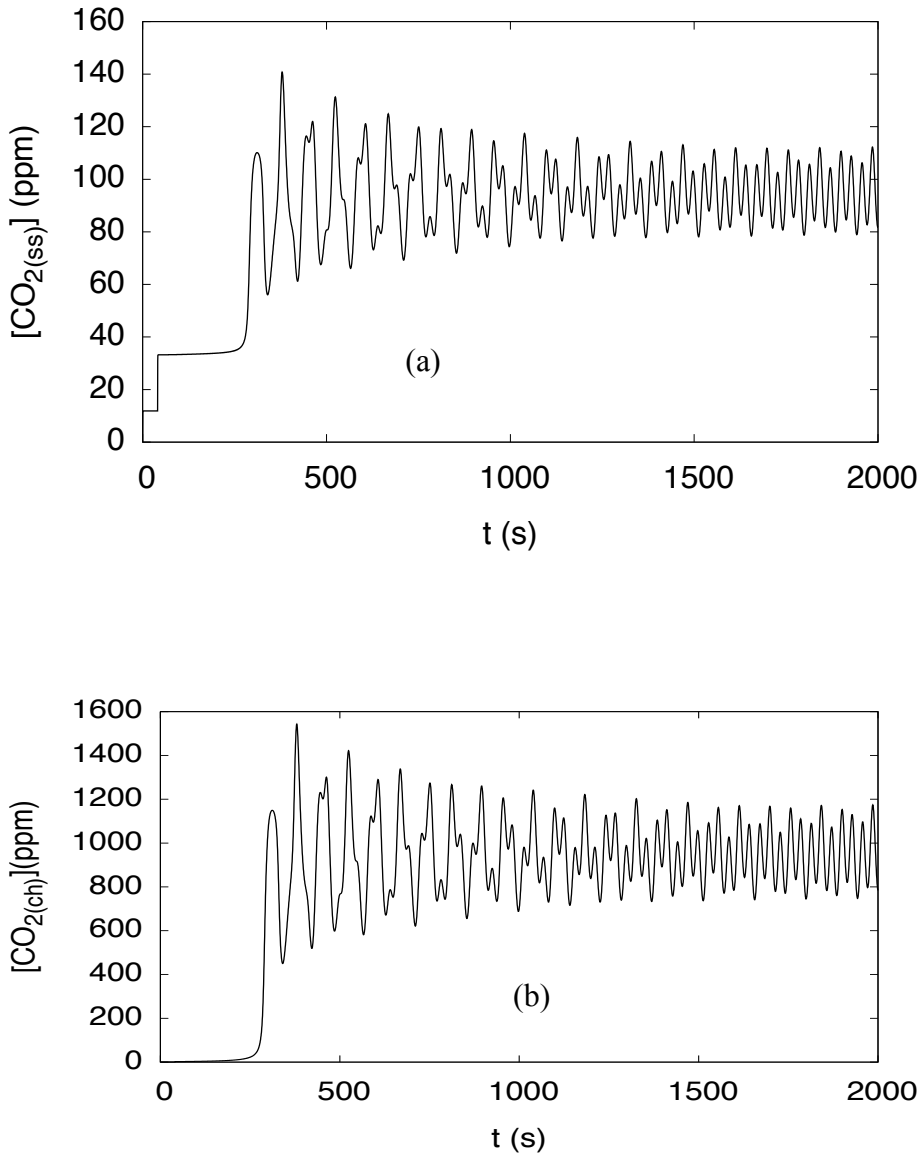

Figure 15: Irregular oscillations of CO_2 in (a) the substomatal space and (b) the chloroplast at the parameter set 1.

As mentioned before, the transient chaotic oscillations do not persist and are transformed into regular oscillations. Figure 16 shows the regular oscillations that are produced in the same parameter set 1. The period and the oscillations range are still slower and higher, respectively. In particular, the oscillation range expanded to 580-1420 ppm of chloroplastic CO_2 concentration (fig 16).

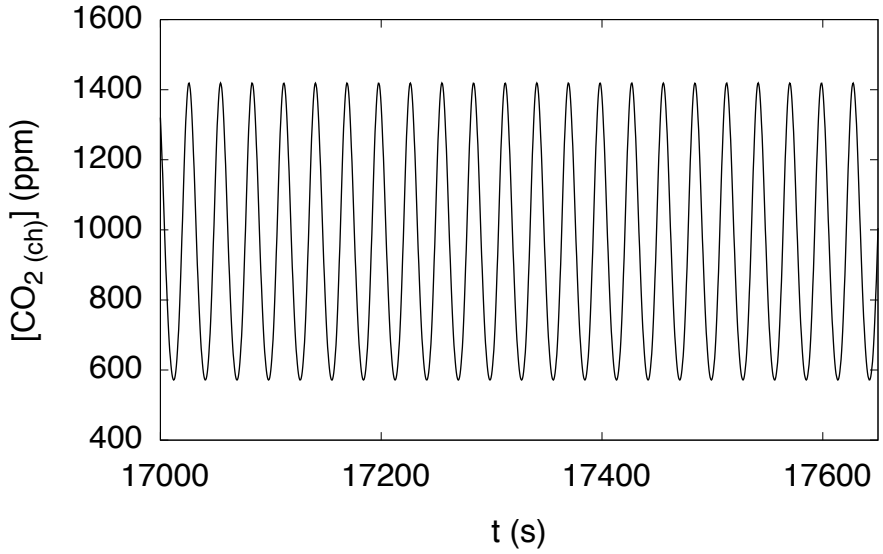

Figure 16: Regular oscillations in the parameter set 1 where some of the parameters are not in the physiological range.

So, the model produced both the irregular and regular oscillations in a non-physiological set of parameters. Furthermore, both the period and range of oscillations were slower and higher respectively compared to the experiment in both types of oscillations. So, our next attempt was finding the oscillations that are compatible with experimental observation in terms of period and range, but in a physiological set of parameters. In doing this, we found that the model produces only the regular oscillations in another set of parameters (termed as non-physiological parameter set 2; Table 3).

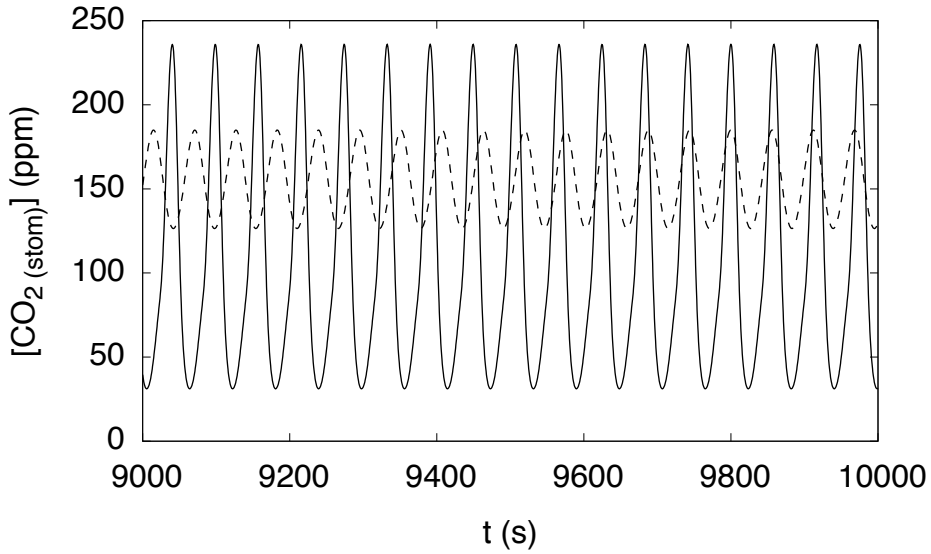

Figure 17: Result of varying the parameter $K_{CO_2,\,cyt/chl}$. The regular oscillations shown as a solid line were produced in the parameter set 2 (Table 3) where $K_{CO_2,\,cyt/chl} = 0.5$. The oscillations shown as a dashed line were produced upon changing $K_{CO_2,\,cyt/chl} = 1.1$.

In this parameter set 2, only the catalytic rate constant ($k_8 = 0.016\ s^{-1}$ in default parameter set) is closer to the physiological catalytic rate constant. But the K_m ratio (4×10^{-5} mM) and the partition coefficient for CO_2 from cytoplasm to mitochondria ($K_{CO_2,\,cyt/mito} = 0.01$) are 1000 times and 10 times smaller respectively compared to the physiological range. Further, the oscillating range is quite wide in range (48-240 ppm) (fig 18) of subtomatal CO_2. But changing two parameters of the parameter set 2 independently could narrow the range of the oscillations. First, a change in the value of the partition coefficient for CO_2 from cytoplasm to chloroplast ($K_{CO_2,\,cyt/chl} = 1.1$) reduces the oscillating range to 130-180 ppm (fig 17). Second, if we only change the k_8 value to $0.0167\ s^{-1}$ the model oscillates within the range 145-155 ppm of substomatal (fig 18 a) and of 64-74 ppm (fig 18 b) of chloroplastic CO_2, where the range of oscillations is about 10 ppm in both compartments that is nearly compatible with experimental observations of about 4 ppm.[8] But the

substomatal CO_2 concentrations are relatively high compared to the experiment. Hence, the model is producing non-physiological behavior in this particular parameter set. The model also produces oscillations in every 50 seconds, which is still very slow compared to the experimental oscillations.[8]

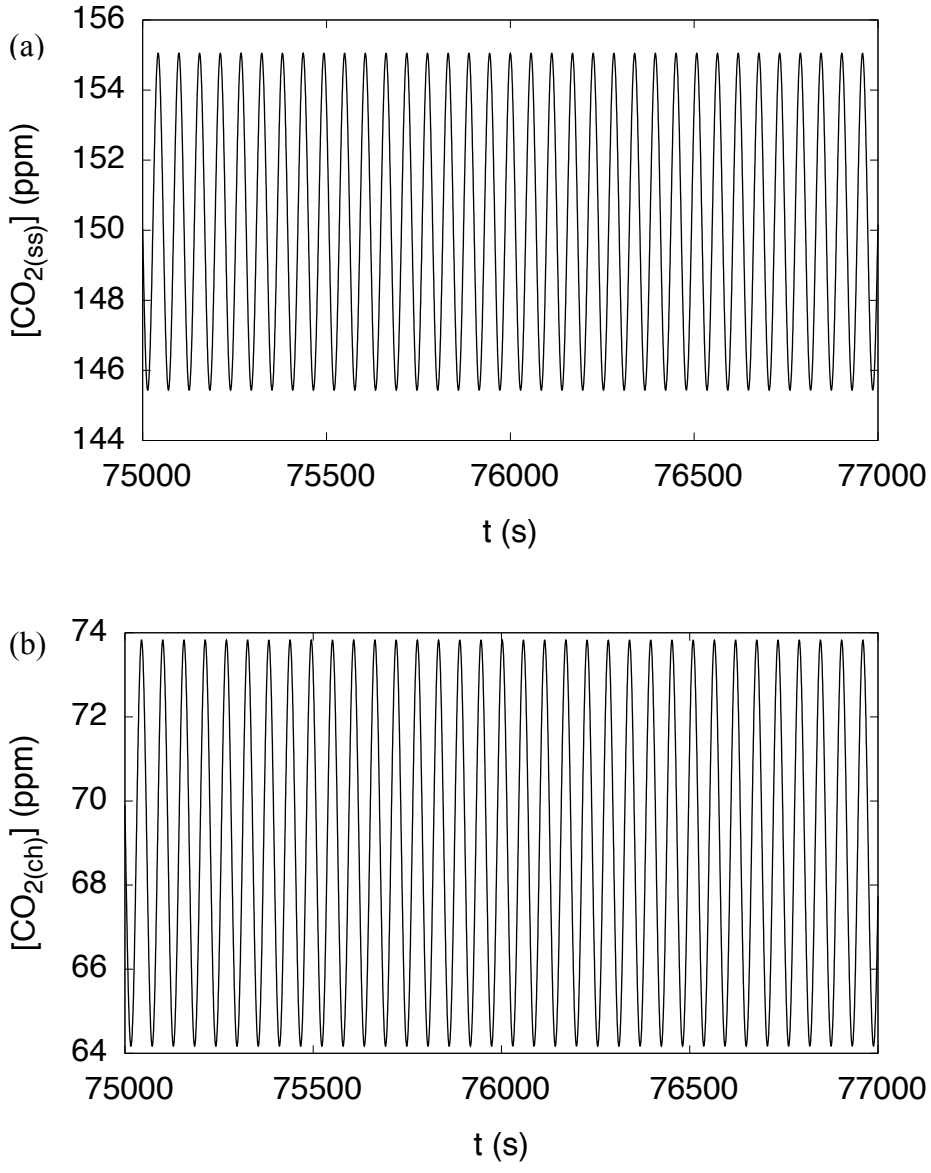

Figure 18: Regular oscillations (a) within the range 145-155 ppm in the substomatal space and (b) 64-74 ppm in the chloroplast at the parameter set 2 (Table 3), with k_8 changed to 0.0167 s^{-1}.

In parameter set 3 (Table 3), the model also produces regular oscillations (fig 19) where $k_8 = 0.003\ s^{-1}$ and $K_{CO_2,\,cyt/ss} = 30$ are not in the physiological range. We would say this parameter set is comparatively in the physiological range compared to other sets of parameters (sets 1 and 2, Table 3). The period of oscillations was slow (~100 s per oscillations) and the range of oscillations of chloroplastic CO_2 was very high (~ 3500 ppm) compared to the oscillations in parameter sets 1 and 2. One other important finding is that in parameter set 3 (physiological range) the model does not produce oscillations at lower values of τ_2 (where $\tau_2 = 270$ s; Table 3) whereas in the parameter sets 1 and 2 (both are in the non-physiological range), the system produces oscillations for $\tau_2 = 40$ s and $\tau_2 = 20$ s respectively (Table 3).

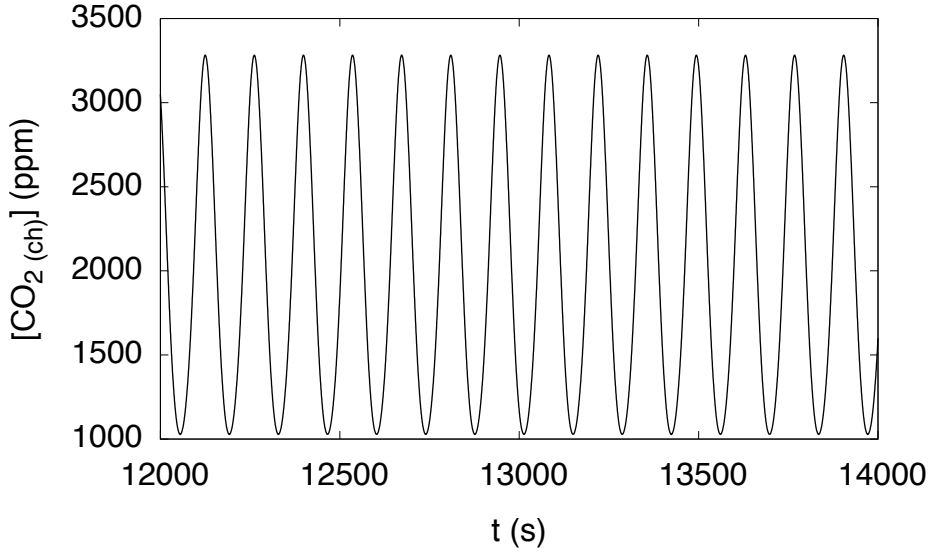

Figure 19: Regular oscillations in the parameter set 3 (Table 3) where most parameters are in the physiological range.

4.3 Atmospheric concentration of CO_2

The model behavior at normal atmospheric CO_2 concentration (about 390 ppm) was verified. The simulated result is shown in fig 20. Damped oscillations were observed at an atmospheric concentration of about 390 ppm. Eventually the system went to the steady state within 10-12 minutes. In contrast, the model exhibited sustained regular oscillations at a lower atmospheric concentration of CO_2 of about 36 ppm. At lower atmospheric CO_2 concentration, sustained oscillations are observed in the experiment[8] as in our model. But again the model produced unreasonably high chloroplastic CO_2 concentration at low atmospheric CO_2. Further, only damped oscillations are observed both *in vivo* [16, 82] and in our model at normal atmospheric CO_2 levels. The period and damping are similar to those observed for photosynthetic oscillations under these conditions[16, 82] and steady-state CO_2 level is similar to that observed *in vivo* as well.[20]

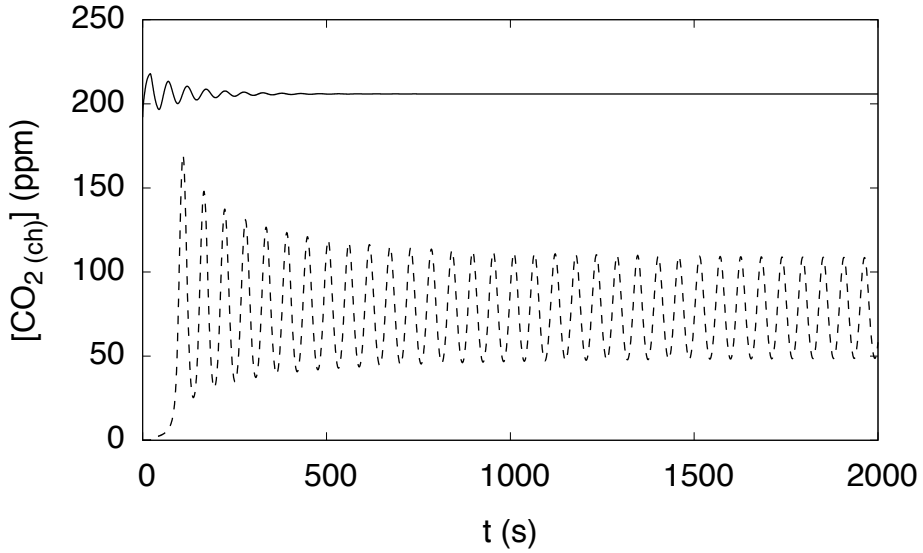

Figure 20: Model behavior at normal atmospheric and low CO_2 concentration; oscillations at high (390 ppm; solid line) and low (36 ppm; dashed line) atmospheric CO_2 concentration at parameter set 2. Oscillations in the high-CO_2 case were started at t=0 by changing the atmospheric CO_2 concentration suddenly to 390 ppm after letting the system reach a steady state with $[CO_2]_{(atm)}$ =350 ppm.

4.3 Bifurcation analysis

How a system responds over time under different conditions (i.e. at different parameter values) can be studied through bifurcation analysis. Bifurcation analysis describes the topological changes of the vector field, that is the qualitative behavior of the model, when we vary parameters.[83-84] Bifurcation analysis was carried out in parameter set 2, because I started working with this parameter set, and completed all bifurcation studies with it for consistency. This bifurcation analysis would be indicative of the bifurcation structure over a wide range of parameters. A bifurcation analysis of the model is presented in figs 21-25.

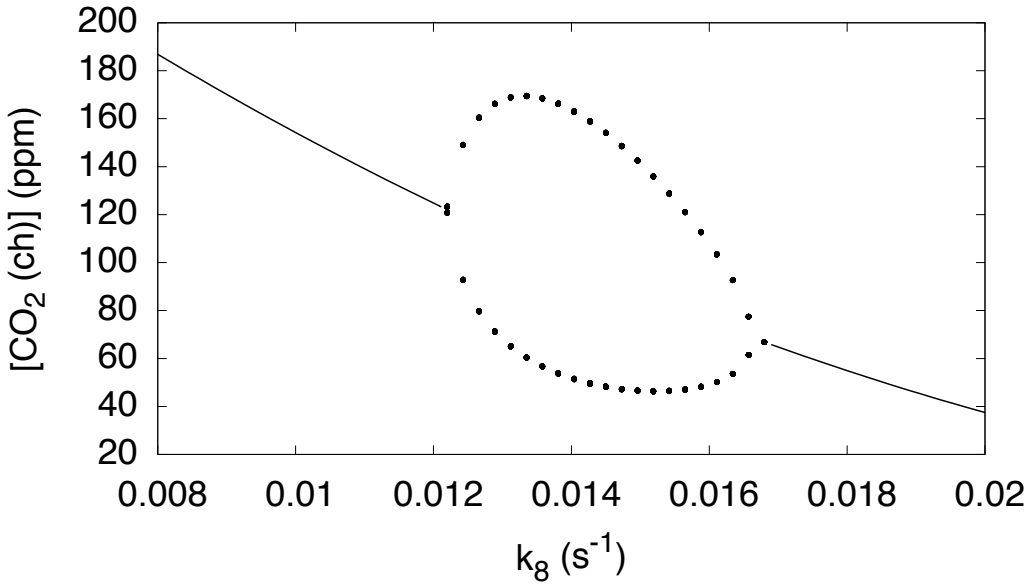

Figure 21: Bifurcation diagram with respect to k_8 at parameter set 2 (Table 3)

Normally, bifurcation diagrams are generated with respect to a parameter of the model plotted along the x-axis. Two dots represent the minima and maxima of the

oscillations. A solid line represents the steady state of the system. In fig 21, the model oscillates within a very limited range of k_8 value (0.0125-0.017 s). Outside this range, the system goes to a steady state. In the oscillating region, the minimum point of the oscillations (50 ppm) is around $k_8 = 0.015\ s^{-1}$, but at the same value of k_8 the maximum point is about 140 ppm. The minimum is close to the experimentally observed oscillations[8] but the maximum is much too high.

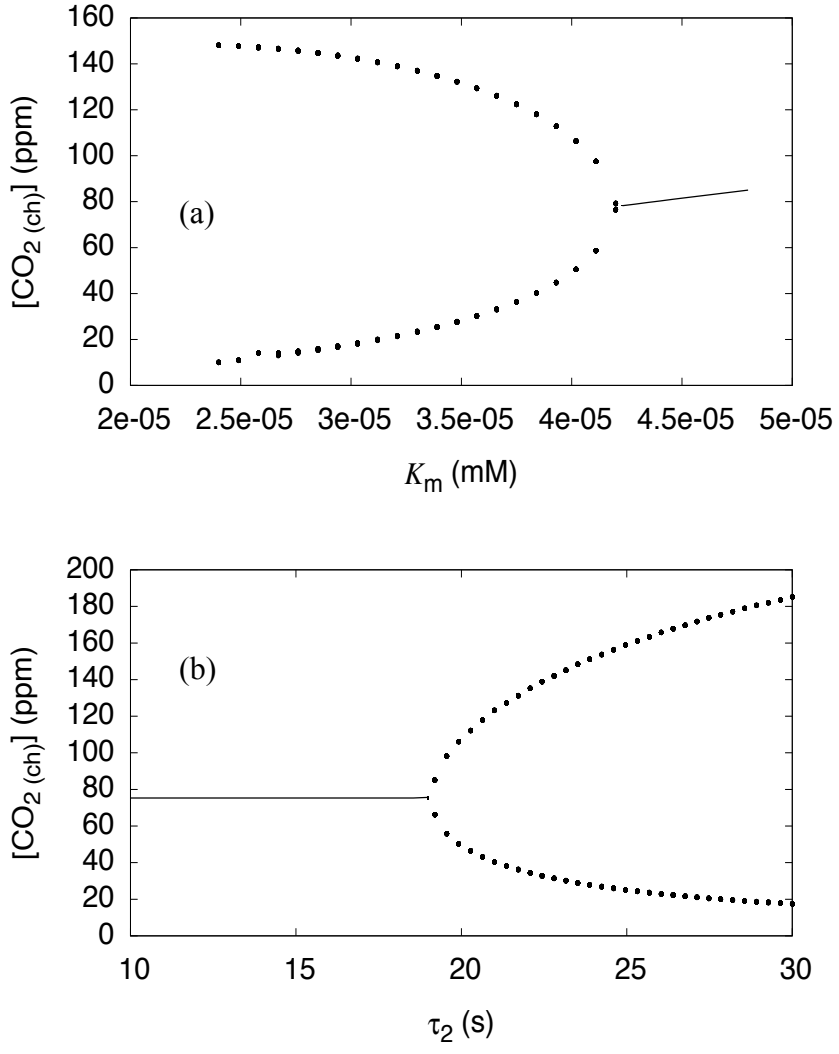

Figure 22: Bifurcation analysis with respect to K_m of the carboxylase reaction (a) and the delay τ_2 (b) at parameter set 2 (Table 3)

The experimentally observed oscillation range was 34-38 ppm of substomatal CO_2.[8] The chloroplastic CO_2 concentration may be of a similar magnitude as the atmospheric CO_2, but it should not be higher.[20] The model is thus seen to produce unrealistically high chloroplastic CO_2 concentrations. As mentioned earlier the model also produces oscillations in a narrower range (64-74 ppm) at $k_8 = 0.0167\ s^{-1}$ (fig 18 and fig 21).

Figure 22 (a) shows the bifurcation analysis with respect to the K_m of the carboxylase reaction. For the parameter set 2 (non-physiological), the K_m value is 4×10^{-5} mM. From the bifurcation diagram, we see that I could make the K_m value somewhat larger in adjusting towards the physiological range. But the minimum of oscillations is going to be shifted to higher chloroplastic CO_2 concentrations. Eventually, the system is transferring to the steady state near the value of 4.3×10^{-5} mM.

Figure 22 (b) shows how the minima and maxima of the oscillations change when varying parameter τ_2. The model transfers from the steady state to the oscillating state at about $\tau_2 = 19.2$ s. The oscillating range increases with increasing τ_2. Physiologically, τ_2 could be in the range of 20-280 s.[47] But if the τ_2 is changed to a larger value the oscillation period will be longer (fig 19) which takes us further from the experimental period of oscillation.[8]

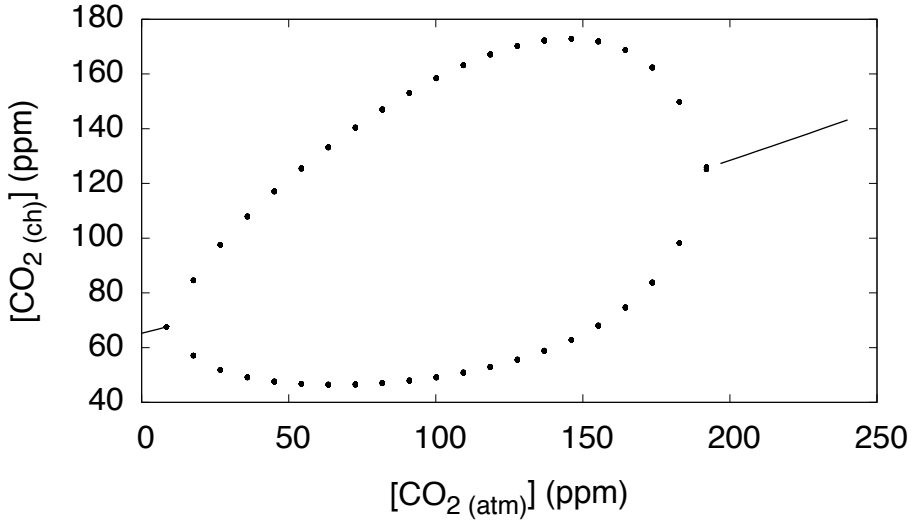

Figure 23: Bifurcation diagram with respect to atmospheric CO_2 concentration at parameter set 2 (Table 3).

The bifurcation analysis with respect to atmospheric CO_2 shows that the system does not oscillate in a high atmospheric CO_2 concentration (above 190 ppm) (fig 23). The system also shifts from the oscillating state to a steady state if the atmospheric CO_2 concentration is below 10 ppm. Normal atmospheric CO_2 concentration is about 390 ppm. The default atmospheric CO_2 concentration in my model is 36 ppm (0.0015 mM), which is the concentration at which the experiments were performed.[8] So, the model displays oscillations at the experimental CO_2 concentration[8] but not at normal ambient CO_2 concentrations, where sustained CO_2 oscillations are not observed.

4.3.1 Bifurcation analysis with respect to the partition coefficients

In parameter set 2, the value of the partition coefficients I used for the analysis are assumptions. The partition coefficient values of different molecules have been

discussed[85] in section 2.2. I tried to keep the values of the partition coefficients in the physiological range. So the bifurcation analysis with respect to these partition coefficients might be useful to assess the range of possible partition coefficients that give oscillations.

Figure 24 (a) shows the bifurcation diagram with respect to the partition coefficient of CO_2 for cytoplasm to substomatal space. In parameter sets 1 and 2, $K_{CO_2,\,cyt/ss}$ is 1, which is not close to the realistic range. This value should be around 0.017 (calculated in section 2.3.3.4). In fig 24 (a), the system stays in a steady state if the $K_{CO_2,\,cyt/ss}$ is less than 1 and starts oscillations if this parameter value is above 1.

Increasing the value of this parameter increases the maximum of the oscillations but the minimum stays constant near to the value of about 30 ppm. This bifurcation diagram shows that the model can only oscillates at larger value of $K_{CO_2,\,cyt/ss}$ compared to the calculated one, which is a fundamental disagreement between model predictions and the experimental result.

The bifurcation analysis with respect to the partition coefficient of CO_2 from cytoplasm to chloroplast shows that the system starts oscillations below about $K_{CO_2,\,cyt/chl} = 1.15$ (fig 24 b). The oscillating amplitude range can be wider if I changed the value of $K_{CO_2,\,cyt/chl}$ to a smaller one. I could have a smaller value of $K_{CO_2,\,cyt/chl}$ to produce oscillations whose minima would be closer to the experimentally observed oscillations,[8] but the maxima would be much higher. A smaller value of $K_{CO_2,\,cyt/chl}$ would indicate that the chloroplast concentrates CO_2 relative to the cytoplasm, which is not realistic for C_3 plants.

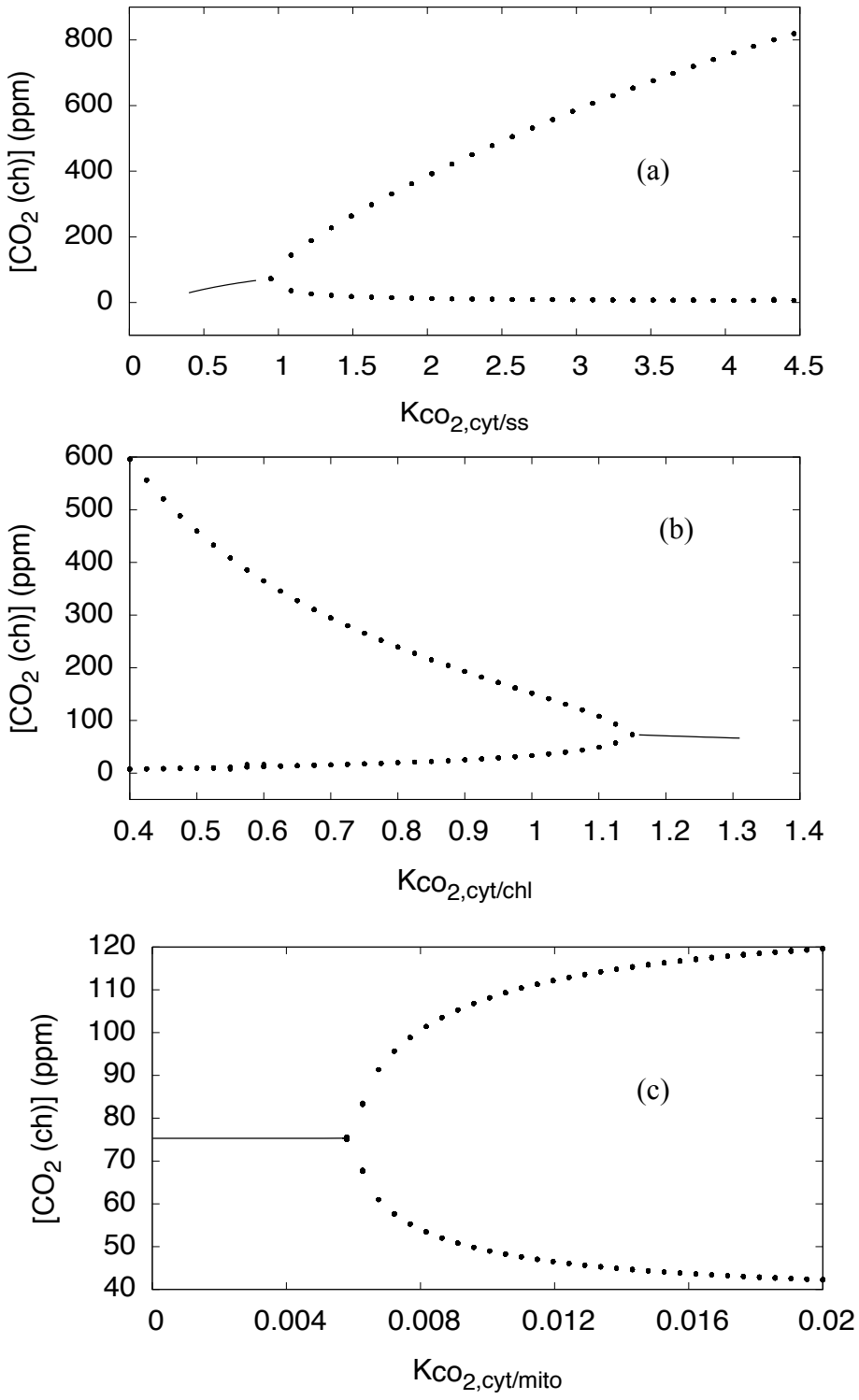

Figure 24: Bifurcation diagram with respect to $K_{CO_2,cyt/ss}$ (a), $K_{CO_2,cyt/chl}$ (b) and $K_{CO_2,cyt/mito}$ (c) at parameter set 2 (Table 3).

In the parameter set 1 (Table 3), $K_{CO_2,\,cyt/chl} = 0.1$, which is comparatively smaller and supports irregular oscillations. This result indicates that the chloroplast may need to accumulate more CO_2 relative to cytoplasm to produce irregular oscillations. But to keep the oscillation range narrow in the regular oscillation mode, which is more consistent with the experimental oscillation range, the $K_{CO_2,\,cyt/chl}$ value was chosen around 1.

The system shifts from a steady state to an oscillating state if the $K_{CO_2,\,cyt/mito}$ value is above 0.006, otherwise staying in a steady state (fig 24 c). The value of $K_{CO_2,\,cyt/mito}$ in parameter sets 1 and 2 is 0.5 and 0.01, respectively, where 0.01 is in a non-physiological range.[48] A larger value of $K_{CO_2,\,cyt/mito} = 0.5$ in parameter set 1 (compared to 0.01 in parameter set 2) implies that the CO_2 is still accumulating in mitochondria but not as much as in parameter set 2, so that unrealistic values of this partition coefficient are not required to support irregular oscillations. With an increasing value of this parameter, the oscillation range spreads (fig 24 c). If the parameter value is in a physiological range of about 1, the oscillating range will be 30-140 ppm, which is quite high (not shown in fig 24 c).

The bifurcation analysis with respect to $K_{O_2,\,cyt/ss}$ shows that the system starts oscillations near the value of 9.7 (fig 25 a). In the oscillating parameter set 2, the $K_{O_2,\,cyt/ss}$ value is set to 10, which is non-physiological. The $K_{O_2,\,cyt/ss}$ value should be around 0.03 (calculated in section 2.3.3.4). But to produce oscillations, large values of $K_{O_2,\,cyt/ss}$ are required. Decreasing the parameter value from 9.6 the system goes to a steady state.

Increasing the parameter value from the steady state, the minima and maxima of oscillations are decreasing slowly and increasing, respectively (fig 25 a).

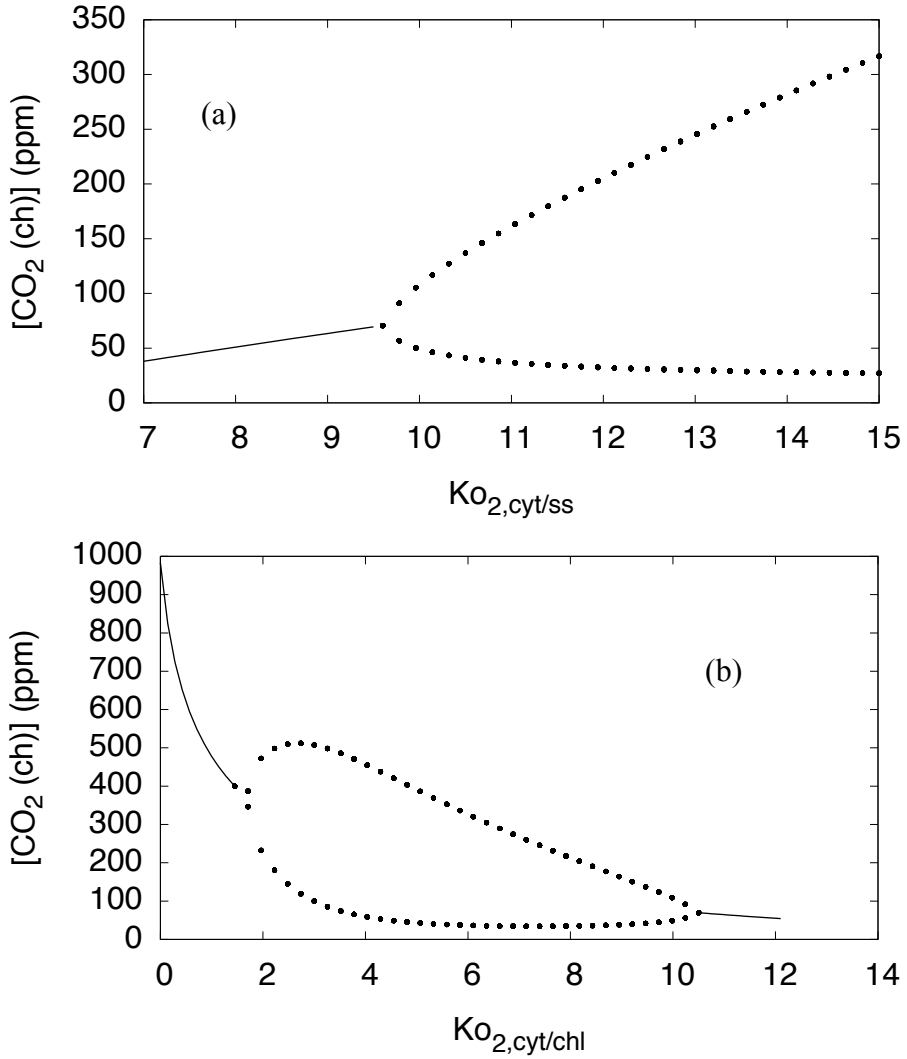

Figure 25: Bifurcation analysis with respect to the partition coefficient of O_2 from cytoplasm to substomatal space (a) and from cytoplasm to chloroplast (b) at parameter set 2 (Table 3).

A range of $K_{O_2,cyt/chl}$ values (1.5-10.5) is described in the fig 25 b, where the system can produce oscillations. With increasing the value of $K_{O_2,cyt/chl}$ from 5 towards 10, the oscillating range decreases from 50-300 ppm to 50-90 ppm. But with increasing the parameter value from 10 to 10.5 the oscillating amplitude range shifted from 50-90 ppm to 60-110 ppm. And if the increasing of the parameter value continues further (10.6-12) the system transfers to a steady state. On the other hand, with decreasing the value of $K_{O_2,cyt/chl}$ from 5 to 1.5, the minima and maxima of the oscillations are shifting from lower to higher chloroplastic CO_2 concentration (from 50-300 ppm to 360-380 ppm), even though the oscillating amplitude range decreases. Eventually, the oscillations die and the system transfers into a steady state (at parameter values lower than 1.5) (fig 25 b).

Chapter 5: Summary and Conclusion

5.1 Summary

A model of photosynthetic oscillations with delay has been developed in this thesis. In this chapter, I will present my conclusions, based on the foregoing mathematical and computational analysis, along with future directions. The major objective of this thesis has been fulfilled, namely the search for oscillations. Presence of at least one critical fragment in the bipartite graph confirms the possibility of oscillations in the model. Furthermore, it is also clear from the mathematical analysis that without delay the model cannot oscillate. The second objective was to reproduce the experimentally observed irregular oscillations through simulations. The model produces both regular and irregular oscillations in different parameter regimes but some of the parameters are not biologically plausible, leading to unrealistically high CO_2 concentrations in the chloroplast and substomatal space, and the oscillations are slower compared to experiment. The conclusion of this study is that recycling of photorespiratory CO_2 is probably not the mechanism for the rapid oscillations observed in the experiment.[8]

5.2 Conclusions

As stated earlier, finding at least one critical fragment in a system is the necessary condition for a model to have the possibility of oscillations. That means a model could have several critical fragments, any of which could support oscillations in a system. Our model's bipartite graph could have more than one critical fragment of higher order. But the critical fragment we found in our model is the only critical fragment of order of six and there are no critical fragments of lower order. The existence of this critical

fragment indicates that the model has the potential for oscillations. Furthermore, the presence of a delay in the model is necessary to make the fragment critical. In other words, the mathematical analysis showed that only the DDE model of the system supports oscillations, i.e. that the oscillations in our model are a delay-induced instability.

The irregular oscillations (fig 15) observed in our simulations (at parameter set 2, non-physiological) are qualitatively compatible with experimental observations. The model showed that the irregular oscillations transformed into regular oscillations in the long run (after 45 minutes). The experimentally observed irregular oscillations were recorded only for 600 s. We don't know what happens after 600 s. The simulated results suggest that the irregular oscillations eventually should transform into regular oscillations if our model is correct. The range and the period of irregular oscillations are not compatible with experimental oscillations. The range of chloroplastic CO_2 concentration during the oscillations is really high, and physiologically not realistic. And the period is much slower (about 25 s) compared to experiment where the system oscillated every few seconds.

There is room for skepticism about the claimed precision of the experimental measurements, which is about 0.1 ppm CO_2,[8] because the measurement of internal CO_2 (C_i) is very much indirect. The C_i measurements rely upon several indirect measurements such as evaporation rate (E), water vapor conductance (g_w) and photosynthetic assimilation rate (A). So, it might be possible that irregular oscillation exists in the system but not in that much faster period (about few seconds) and narrower range (2-4

ppm), which was observed in the experiment.[8] Another experimental measurement of internal CO_2 of tobacco leaves with longer run time compared to the performed experiment (where the run time was only 10 minutes)[8] would be worthwhile. Further, the repetition of the experiment might confirm whether the transient irregular oscillations observed in our simulations (fig 15) are possible or not in real plant life.

One important thing is that the parameter set 1 (Table 3) that supports the irregular oscillations is not even close to a realistic parameter set. An effort was made to fix the range and period of oscillations in a more realistic parameter set. First, I tried to produce the irregular oscillations with a realistic parameter set. That was unsuccessful. Interestingly, I observed that the oxygenase reaction kinetics (particularly the catalysis rate of the oxygenase) needed to be faster compared to the default parameter value (table 2) to support the irregular oscillations. This makes sense because an increase in the catalysis rate of the oxygenase reaction supports the production of CO_2 in the mitochondria that in turns raises the CO_2 in chloroplast, which favors the carboxylase reaction. This mechanism of switching reactions between the carboxylase and oxygenase can support oscillations.

Efforts were also made towards fixing the period and range of the regular oscillations produced (at parameter set 2, non-physiological), which were partially successful. The range of regular oscillations (10 ppm, fig 18 a) produced in our simulations is not dissimilar to the experimental range of 4 ppm[8] although the absolute concentrations are too high. Moreover, the period is a lot larger (50 s / oscillation) compared to experiment

(few seconds / oscillation). Finally, we were able to generate regular oscillations in our simulations at the parameter set 3 (reasonably physiological compared to other two parameter sets). But the period is way larger (about 100 s) and the range is quite high (fig 19), which is biologically not realistic.

Bifurcation analyses with respect to some of the parameters have been performed (figs 21-25), which show how changes in the parameter value influence the dynamics of the model. Among other things, these analyses reveal how much change in a parameter value can take place while maintaining the oscillation phenomenon. The bifurcation analyses made in this thesis did not uncover a parameter regime where I could fulfill all aspects of the experimental oscillations[8] or where all the parameters were in the physiological range, for that matter.

Our results are compatible with the modeling study of Dubinsky and Ivlev[17] where they also found regular oscillations. They found oscillation amplitudes of 2-6 ppm and a period of 1 s / oscillation, which is more compatible with experimental findings. But their model is over-simplified in terms of biochemical detail (reviewed in section 1.6). Furthermore, irregular oscillations were not observed in their model. On the other hand, a reasonably realistic model is built in my thesis where diffusion and partition coefficients of gases among compartments have been taken account. Unfortunately we could not find some of the characteristic behaviors (irregular oscillations of correct period and with realistic CO_2 concentrations) in the physiological range. These results suggest that the experimentally observed oscillations are not due to recycling of photorespiratory CO_2.

It might be possible that some pieces of important biochemistry are missing in our version of the model. So, the addition of biochemical details of the conversion chemistry of P-glycolate to CO_2 to this model might be one future direction for this project. As already mentioned, the conversion of P-glycolate to CO_2 and serine takes place in the chloroplast, peroxisome and mitochondria compartments of a leaf. This process is quite complex but worthwhile to combine with this model in an effort to fix the period and to bring the value of some of the parameters into a realistic range.

References

1. Ingenhousz, J., Experiments Upon Vegetables: Discovering their great power of puryfying the common air in the sunshine. *The Critical Review, Or, Annals of Literature* **1779,** *48*, 334.

2. Prinn, R. G.; Reilly, J. M.; Sarofim, M. C.; Wang, C.; Felzer, B. S., Effects of Air Pollution Control on Climate. *In: Schlesinger, M. (Ed.), Integrated Assessment of Human-induced Climate Change. Cambridge University Press, Cambridge, UK (in press), and MIT Joint Program for the Science and Policy of Global Change.* **2007,** *Report No. 118, January 2005, Cambridge, MA.*

3. Wingler; Astrid and Lea; Peter John and Quick; Paul, W.; Leegood, R. C., Photorespiration: Metabolic pathways and their role in stress protection. *Philosophical Transactions of the Royal Society of London Series B - Biological Sciences* **2000,** *355* (1402), 1517-1529.

4. Bauwe, H., Recent developments in photorespiration research. . *Biochemical Society Transactions* **2010** *038* (2), 677-682.

5. Rachmilevitch, S.; Cousins, A. B.; Bloom, A. J., Nitrate assimilation in plant shoots depends on photorespiration. *Proceedings of the National Academy of Sciences* **2004,** *101* (31), 11506-11510.

6. Cegelski, L.; Schaefer, J., NMR determination of photorespiration in intact leaves using in vivo $^{13}CO_2$ labeling. *Journal of Magnetic Resonance* **2006,** *178* (1), 1-10.

7. Laisk, A.; Sumberg, A., Partitioning of the leaf CO_2 exchange into components using CO_2 exchange and fluorescence measurements. *Plant Physiology.* **1994,** *106* (2), 689-695.

8. Roussel, M. R.; Alexander A I; Igamberdiev, A. U., Oscillations of the internal CO_2 concentration in tobacco leaves transferred to low CO_2. *Journal of Plant Physiology* **2007,** *164* (9), 1188-1196.

9. Poolman, M. G.; Assmus, H. E.; Fell, D. A., Applications of metabolic modelling to plant metabolism. *Journal of Experimental Botany* **2004,** *55* (400), 1177-1186.

10. Doedel, E. J., AUTO, a program for the automatic bifurcation analysis of autonomous systems. *Cong. Numer.* **1981,** *30*, 265-384.

11. Albers, E.; Bakker, B. M.; Gustafsson, L., Modeling response of glycolysis in *S. cerevisiae* cells harvested at diauxic shift. *Molecular Biology Reports* **2002,** *29* (1), 119-123.

12. Mendes, P., Gepasi: a software package for modelling the dynamics, steady states and control of biochemical and other systems. *Computer Applications in the Biosciences* **1993,** *9* (5), 563-571.

13. Teruo, O., Simple oscillations in photosynthesis of higher plants. *Biochimica et Biophysica Acta (BBA) - Bioenergetics* **1982,** *681* (1), 103-109.

14. Walker, D. A.; Sivak, M.; Prinsley, R.; Cheesbrough, J., Simultaneous measurement of oscillations in oxygen evolution and chlorophyll a fluorescence in leaf pieces. *Plant Physiology.* **1983,** *73(3)*, 542–549.

15. Laisk, A.; Siebke, K.; Gerst, U.; Eichelmann, H.; Oja, V.; Heber, U., Oscillations in photosynthesis are initiated and supported by imbalances in the supply of ATP and NADPH to the Calvin cycle. *Planta* **1991,** *185* (4), 554-562.

16. Rovers, W.; Giersch, C., Photosynthetic oscillations and the interdependence of photophosphorylation and electron transport as studied by a mathematical model. *Biosystems* **1995,** *35* (1), 63-73.

17. Dubinsky, A. Y.; Ivlev, A. A., Computational analysis of the oscillatory dynamics in the processes of CO_2 assimilation and photorespiration. *Biosystems* **2011,** *103* (2), 285-290.

18. Roussel, M., Slowly reverting enzyme inactivation: a mechanism for generating long-lived damped oscillations. *Journal of Theoretical Biology* **1998,** *195* (2), 233-244.

19. Jones, H. G., Physicochemical and Environmental Plant Physiology, 2nd edn. *Journal of Applied Ecology* **1999,** *36* (6), 1076-1077.

20. Williams, T. G.; Flanagan, L. B.; Coleman, J. R., Photosynthetic gas exchange and discrimination against $^{13}CO_2$ and $C^{18}O^{16}O$ in tobacco plants modified by an antisense construct to have low chloroplastic carbonic anhydrase. *Plant Physiology.* **1996,** *112* (1), 319-326.

21. Brooks, J. R.; Flanagan, L. B.; Varney, G. T.; Ehleringer, J. R., Vertical gradients in photosynthetic gas exchange characteristics and refixation of respired CO_2 within boreal forest canopies. *Tree Physiology* **1997,** *17* (1), 1-12.

22. Roy, H.; Andrews, T., Rubisco: assembly and mechanism. In:Leegood, R. Sharkey, T. von Caemmerer, S. (eds), Photosynthesis: physiology and metabolism. **2000**, 53-83.Kluwer Academic Publisher, Netherland.

23. Foyer, C. H.; Bloom, A. J.; Queval, G.; Noctor, G., Photorespiratory metabolism: genes, mutants, energetics, and redox signaling. *Annual Review of Plant Biology* **2009,** *60* (1), 455-484.

24. Spreitzer, R. J.; Salvucci, M. E., Rubisco: Structure, regulatory interactions, and possibilities for a better enzyme. *Annual Review of Plant Biology* **2002,** *53* (1), 449-475.

25. Mueller-Cajar, O.; Badger, M. R., New roads lead to Rubisco in archaebacteria. *BioEssays* **2007,** *29* (8), 722-724.

26. Yeoh, H. H.; Badger, M. R.; Watson, L., Variations in K_m (CO_2) of ribulose-1,5-bisphosphate carboxylase among grasses. *Plant Physiology.* **1980,** *66* (6), 1110-1112.

27. Lorimer George H.; Murray R. Badger; Andrews, T. J., The activation of ribulose-1,5-bisphosphate carboxylase by carbon dioxide and magnesium ions. Equilibria, kinetics, a suggested mechanism, and physiological implications. *Biochemistry* **1976** *15* (3), 529-536.

28. Pierce, J.; Lorimer, G. H.; Reddy, G., Kinetic mechanism of ribulosebisphosphate carboxylase: evidence for an ordered, sequential reaction. *Biochemistry* **1986,** *25* (7), 1636-1644.

29. Jordan, D.; Ogren, W., Species variation in kinetic properties of ribulose 1,5-bisphosphate carboxylase/oxygenase. *Archives of Biochemistry and Biophysics* **1983,** *227*, 425-433.

30. Bainbridge, G.; Madgwick, P.; Parmar, S.; Mitchell, R.; Paul, M.; Pitts, J.; Keys, A. J.; Parry, M. A. J., Engineering Rubisco to change its catalytic properties. *Journal of Experimental Botany* **1995,** *46* (special issue), 1269-1276.

31. RW Pearcy; JP Krall; GF Sassenrath-Cole, In: Baker NR (ed) Photosynthesis and the environment. **1996**, 321-346. Kluwer Academic Publisher, Dordrecht.

32. Von Caemmerer, S.; Paul, Q. W., Rubisco: Physiology in vivo. In : Richard C. Leegood, Thomas D. Sharkey, Susanna von Caemmerer (eds), Photosynthesis: physiology and metabolism. **2000**, 86-113. Kluwer Academic Publisher, Netherland.

33. Hammond, E. T.; Andrews, T. J.; Mott, K. A.; Woodrow, I. E., Regulation of Rubisco activation in antisense plants of tobacco containing reduced levels of Rubisco activase. *The Plant Journal* **1998,** *14*, 101–110.

34. Mott, K. A.; Snyder, G. W.; Woodrow, I. E., Kinetics of Rubisco activation as determined from gas-exchange measurements in antisense plants of *Arabidopsis thaliana* containing reduced levels of Rubisco activase. *Functional Plant Biology* **1997,** *24* (6), 811-818.

35. Salvucci, M.; Ogren, W., The mechanism of Rubisco activase: Insights from studies of the properties and structure of the enzyme. *Photosynthesis Research* **1996,** *47*, 1-11.

36. Portis, A. R., The regulation of Rubisco by Rubisco activase. *Journal of Experimental Botany* **1995,** *46* (special issue), 1285-1291.

37. Seemann, J.; Sharkey, T.; Wang, J.; CB., O., Environmental effects on photosynthesis, nitrogen-use efficiency, and metabolite pools in leaves of sun and shade plants. *Plant Physiology.* **1987,** *84*, 796–802.

38. Price, G.; Evans, J.; Caemmerer, S.; Yu, J.; Badger, M., Specific reduction of chloroplast glyceraldehyde-3-phosphate dehydrogenase activity by antisense RNA reduces CO_2 assimilation via a reduction in ribulose bisphosphate regeneration in transgenic tobacco plants. *Planta* **1995,** *195*, 369-378.

39. Yeoh, H.-H.; Badger, M. R.; Watson, L., Variations in kinetic properties of ribulose-1,5-bisphosphate carboxylases among plants. *Plant Physiology.* **1981,** *67* (6), 1151-1155.

40. Farquhar, G., Models describing the kinetics of ribulose biphosphate carboxylase-oxygenase. *Archives of Biochemistry and Biophysics* **1979,** *193*, 456-468.

41. Laing, W.; Christeller, J., A model for the kinetics of activation and catalysis of ribulose 1,5-bisphosphate carboxylase. *Biochemical Journal.* **1976,** *159*, 563–570.

42. R Douce; H W Heldt, Photorespiration. In : Richard C. Leegood, Thomas D. Sharkey, Susanna Von Caemmerer (eds), Photosynthesis: physiology and metabolism **2000**, 115-136. Kluwer Academic Publisher, Netherland.

43. Husic, D. W.; Husic, H. D.; Tolbert, N. E.; Black, C. C., The oxidative photosynthetic carbon cycle or C_2 cycle. *Critical Reviews in Plant Sciences* **1987,** *5* (1), 45 - 100.

44. David Hondred; Dawn-Marie Wadle; David E. Titus; Becker, W. M., Light-stimulated accumulation of the peroxisomal enzymes hydroxypyruvate reductase and serine:glyoxylate aminotransferase and their translatable mRNAs in cotyledons of cucumber seedlings. *Plant Molecular Biology* **1987,** *9* (3), 259-275.

45. T Noguchi; S Hayashi, Plant leaf alanine: 2-oxoglutarate aminotransferase. Peroxisomal localization and identity with glutamate:glyoxylate aminotransferase. *Biochemical Journal* **1981** *195* (1), 235–239.

46. Winkel, B. S. J., Metabolic channeling in plants. *Annual Review of Plant Biology* **2004,** *55* (1), 85-107.

47. Atkin, O.; Millar, A.; Gardeström, P.; Day, D., Photosyntesis, carbohydrate metabolism and respiration in leaves of higher plants. In: Leegood, R. Sharkey, T. Caemmerer, S. (eds), Photosynthesis: physiology and metabolism. **2000**, 153-175.Kluwer Academic Publisher, Netherland.

48. Nobel, P., Leaves and fluxes. In:Physicochemical and environmental plant physiology. *4th edition* **2009**, 293-337.

49. Allan, W. L.; Clark, S. M.; Hoover, G. J.; Shelp, B. J., Role of plant glyoxylate reductases during stress: a hypothesis. *Biochemical Journal* **2009,** *423* (1), 15-22.

50. Kleczkowski, L. A.; Edwards, G. E.; Blackwell, R. D.; Lea, P. J.; Givan, C. V., Enzymology of the reduction of hydroxypyruvate and glyoxylate in a mutant of barley lacking peroxisomal hydroxypyruvate reductase. *Plant Physiology.* **1990,** *94* (2), 819-825.

51. Murray, A. J. S.; Blackwell, R. D.; Lea, P. J., Metabolism of hydroxypyruvate in a mutant of barley lacking NADH-dependent hydroxypyruvate reductase, an important photorespiratory enzyme activity. *Plant Physiology.* **1989,** *91* (1), 395-400.

52. Flügge, U.-l., Metabolite transport across the chloroplast envelope of C_3 plants. In: Leegood, R. Sharkey, T. Caemmerer, S. (eds), Photosynthesis: Physiology and metabolism, . **2000**, 137-152. Kluwer Academic Publisher, Netherland.

53. Fischer, K.; Arbinger, B.; Kammerer, B.; Busch, C.; Brink, S.; Wallmeier, H.; Sauer N; Eckerskorn, C.; Ulf-Ingo Flügge, Cloning and in vivo expression of functional triose phosphate/phosphate translocators from C_3- and C_4-plants: evidence for the putative participation of specific amino acid residues in the recognition of phosphoenolpyruvate. *The Plant Journal* **1994,** *5* (2), 215-226.

54. Brink, S.; Fischer, K.; Klosgen, R. B.; Flugge, U. I., Sorting of nuclear-encoded chloroplast membrane proteins to the envelope and the thylakoid membrane. *Journal of Biological Chemistry* **1995,** *270* (35), 20808-20815.

55. Roussel, M. R., The Use of delay differential equations in chemical kinetics. *The journal of physical chemistry* **1996,** *100* (20), 8323-8330.

56. Roussel, C. J.; Roussel, M. R., Delay-differential equations and the model equivalence problem in chemical kinetics. *Physics in Canada* **2001,** *57*, 114–120.

57. Nobel, P., Cells and diffusion. In: Physicochemical and environmental plant physiology. *4th edition* **2009**, 1-25.

58. Leo, A.; Hansch, C.; Elkins, D., Partition coefficients and their uses. *Chemical Reviews* **1971,** *71* (6), 525-616.

59. Servaites, J. C., Crystalline ribulose bisphosphate carboxylase/oxygenase of high integrity and catalytic activity from Nicotiana tabacum. *Archives of Biochemistry and Biophysics.* **1985,** *238* (1), 154-60.

60. Brian, J. A.; Paul, E. K.; Colin, G. N. T., Carbon dioxide assimilation and respiration. *Plants in Action: Adaptation in Nature, Performance in Cultivation* **1999**, 62.
61. Stroppolo, M.; Falconi, M.; Caccuri, A.; Desideri, A., Superefficient enzymes. *Cellular and Molecular Life Sciences* **2001,** *58* (10), 1451-60.

62. Hahn, B. D., A Mathematical model of photorespiration and photosynthesis. *Annals of Botany* **1987,** *60* (2), 157-169.

63. Pickersgill, R. K., An upper limit to the active site concentration of ribulose bisphosphate carboxylase in chloroplasts. *Biochemical Journal* **1986,** *236* (1), 311.

64. Hitz, W. D.; Stewart, C. R., Oxygen and Carbon Dioxide Effects on the Pool Size of Some Photosynthetic and Photorespiratory Intermediates in Soybean (*Glycine max* [L.] Merr.). *Plant Physiology.* **1980,** *65* (3), 442-446.

65. Winter, H.; Robinson, D.; Heldt, H., Subcellular volumes and metabolite concentrations in spinach leaves. *Planta* **1994,** *193* (4), 530-535.

66. Jensen, R. G.; Bahr, J. T., Ribulose 1,5-bisphosphate carboxylase-oxygenase. *Annual Review of Plant Physiology* **1977,** *28* (1), 379-400.

67. Von Caemmerer, S.; Evans, J. R.; Hudson, G. S.; Andrews, T. J., The kinetics of ribulose-1,5-bisphosphate carboxylase/oxygenase *in vivo* inferred from measurements of photosynthesis in leaves of transgenic tobacco. *Planta* **1994,** *195* (1), 88-97.

68. Farazdaghi, H., The single-process biochemical reaction of Rubisco: A unified theory and model with the effects of irradiance, CO_2 and rate-limiting step on the kinetics of C_3 and C_4 photosynthesis from gas exchange. *Biosystems* **2011,** *103* (2), 265-284.

69. Garrett, M. K., Control of photorespiration at RuBP carboxylase/oxygenase level in ryegrass cultivars. *Nature* **1978,** *274* (5674), 913-915.

70. Lan, Y.; Mott, K. A., Determination of apparent K_m values for ribulose 1,5-bisphosphate carboxylase/oxygenase (Rubisco) activase using the spectrophotometric assay of Rubisco activity. *Plant Physiology.* **1991,** *95* (2), 604-609.

71. Lawlor, D. W., A semi quantitative analysis of the photosynthetic system in an average C_3 plant leaf. *Photosynthesis: Molecular,Physiological and Enviromental Processes; 3rd eds* **2001**, 56.

72. Uehlein, N.; Otto, B.; Hanson, D. T.; Fischer, M.; McDowell, N.; Kaldenhoff, R., Function of *Nicotiana tabacum* Aquaporins as Chloroplast Gas Pores Challenges the Concept of Membrane CO_2 Permeability. *The Plant Cell Online* **2008,** *20* (3), 648-657.

73. Gorton, H. L.; Herbert, S. K.; Vogelmann, T. C., Photoacoustic analysis indicates that chloroplast movement does not alter liquid-phase CO_2 diffusion in leaves of *Alocasia brisbanensis*. *Plant Physiology* **2003,** *132* (3), 1529-1539.

74. Carroll, J. J.; Mather, A. E., The system carbon dioxide-water and the Krichevsky-Kasarnovsky equation. *Journal of Solution Chemistry* **1992,** *21* (7), 607-621.

75. Mincheva, M.; Roussel, M., Graph-theoretic methods for the analysis of chemical and biochemical networks. I. Multistability and oscillations in ordinary differential equation models. *Journal of Mathematical Biology* **2007,** *55* (1), 61-86.

76. Mincheva, M.; Roussel, M., Graph-theoretic methods for the analysis of chemical and biochemical networks. II. Oscillations in networks with delays. *Journal of Mathematical Biology* **2007,** *55* (1), 87-104.

77. Clarke, B. L., Graph theoretic approach to the stability analysis of steady state chemical reaction networks. *The Journal of Chemical Physics* **1974,** *60* (4), 1481-1492.

78. Clarke, B. L., Stability analysis of a model reaction network using graph theory. *The Journal of Chemical Physics* **1974,** *60* (4), 1493-1501.

79. Clarke, B. L., Theorems on chemical network stability. *The Journal of Chemical Physics* **1975,** *62* (3), 773-775.

80. Ivanova, A. N.; Tarnopolskii, B. L., one approach to the determination of a number of qualitative features in the behavior of kinetics systems and realization of this approach in a computer (critical conditions, autooscillations). *Kinet. Katal.* **1979,** *20*, 1541-1548.

81. Ermentrout, B.; Author; Mahajan, A., Simulating, analyzing, and animating dynamical systems: A guide to XPPAUT for researchers and students. *Applied Mechanics Reviews* **2003,** *56* (4), B53-B53.

82. Walker, D. A., Concerning oscillations. *Photosynthesis Research* **1992,** *34* (3), 387-395.

83. Borisyuk, R.; Kirillov, A., Bifurcation analysis of a neural network model. *Biological Cybernetics* **1992,** *66* (4), 319-325.

84. Kitano, H., Systems biology: A brief overview. *Science* **2002,** *295* (5560), 1662-1664.